$Li_{1.3}Al_{0.3}Ti_{1.7}(PO_4)_3$ AS A SOLID STATE LI-ION CONDUCTOR: ISSUES WITH MICROCRACKING AND STABILITY IN AQUEOUS SOLUTIONS

by

Spencer D. Jackman

A thesis submitted to the faculty of
The University of Utah
in partial fulfillment of the requirements for the degree of

Master of Science

Department of Materials Science and Engineering

The University of Utah

December 2012

ProQuest LLC.
789 East Eisenhower Parkway
P.O. Box 1346
Ann Arbor, MI 48106 - 1346

The University of Utah Graduate School

STATEMENT OF THESIS APPROVAL

The thesis of **Spencer D. Jackman**

has been approved by the following supervisory committee members:

Raymond A. Cutler	, Chair	**09/26/2012** Date Approved
Anil V. Virkar	, Member	**09/26/2012** Date Approved
Dinesh K. Shetty	, Member	**09/26/2012** Date Approved

and by **Feng Liu** , Chair of

the Department of **Materials Science and Engineering**

and by Charles A. Wight, Dean of The Graduate School.

ABSTRACT

Lithium aluminum titanium phosphate (LATP) with formula $Li_{1.3}Al_{0.3}Ti_{1.7}(PO_4)_3$ was analyzed and tested to better understand its applicability as a solid state ion conducting ceramic material for electrochemical applications. Sintered samples were obtained from Ceramatec, Inc. in Salt Lake City and characterized in terms of density, phase-purity, fracture toughness, Young's modulus, thermal expansion behavior, mechanical strength, a.c. and d.c. ionic conductivity, and susceptibility to static and electrochemical corrosion in aqueous Li salt solutions. It was shown that LATP is prone to microcrack generation because of high thermal expansion anisotropy.

A.c. impedance spectra of high-purity LATP of varying grain sizes showed that microcracking had a negative impact on the ionic conduction of Li along grain boundaries, with fine-grained (1.7±0.7 μm) LATP having twice the ionic conductivity of the same purity of coarse-grained (4.8±1.9 μm) LATP at 50°C. LATP with detectible secondary phases had lower ionic conductivity for similar grain sizes, as would be expected. The Young's modulus of fine-grained LATP was measured to be 115 GPa, and the highest biaxial strength was 191±11 MPa when tested in mineral oil, 144±13 MPa as measured in air, and 26±7 MPa after exposure to deionized water, suggesting that LATP undergoes stress-corrosion cracking. After exposure to LiOH, the strength was 76±19 MPa. This decrease in strength was observed despite there being no measureable change

in a.c. impedance spectra, X-ray diffraction, or sample mass, suggesting phosphate glasses at grain boundaries.

The chemical and electrochemical stability of high-purity LATP in aqueous electrochemical cells was evaluated using LiOH, LiCl, $LiNO_3$, and $LiCOOCH_3$ salts as the Li source. LATP was found to be most stable between pH 8–9, with the longest cell operating continuously at 25 mA cm^{-2} for 625 hours at 40°C in $LiCOOCH_3$. At pH values outside of the 7–10 range, eventual membrane degradation was observed in all aqueous systems under electrochemical conditions. While LATP was surprisingly resistant to static corrosion in a hot, aqueous LiOH solution, electrochemical degradation was observed at the cathode due to subsurface pitting. Strength measurements were more instructive than impedance measurements in detecting this degradation.

TABLE OF CONTENTS

ABSTRACT.....iii

ACKNOWLEDGEMENTS.....vii

1. INTRODUCTION.....1

1.1 Background.....1
1.2 References.....4

2. EFFECT OF MICROCRACKING ON IONIC CONDUCTIVITY OF LATP…...9

2.1 Abstract.....9
2.2 Introduction.....10
2.3 Experimental.....13
2.3.1 Phase-Purity and Characterization of Physical and Mechanical Properties.13
2.3.2 Ionic Conductivity Measurements.....16
2.4 Results and Discussion.....17
2.4.1 Phase-Purity, Physical and Mechanical Properties.....17
2.4.2 Ionic Conductivity.....27
2.5 Conclusions.....31
2.6 References.....33

3. STABILITY OF NASICON-TYPE $Li_{1.3}Al_{0.3}Ti_{1.7}P_3O_{12}$ IN AQUEOUS SOLUTIONS.....37

3.1 Abstract.....37
3.2 Introduction.....38
3.3 Experimental.....39
3.3.1 Characterization of Physical Properties.....39
3.3.2 Static Corrosion Measurements 40
3.3.3 Ionic Conductivity Measurements.....40
3.3.3.1 A.c. Conductivity.....40
3.3.3.2 D.c. Conductivity.....41
3.3.4 Strength Measurements 42
3.4 Results.....43
3.4.1 Physical Properties.....43
3.4.2 Static Corrosion Results.....45
3.4.3 Ionic Conductivity Results.....47

3.4.3.1 A.c. Conductivity....47
3.4.3.2 D.c. Conductivity....49
3.4.4 Strength Results....56
3.5 Discussion....57
3.6 Conclusions....62
3.7 References....63

4. SUMMARY AND CONCLUSIONS....68

4.1 Microcracking....68
4.2 Strength Degradation in Presence of Moisture....69
4.3 LATP as a Solid Electrolyte in Aqueous Media....70

ACKNOWLEDGEMENTS

This work was performed at Ceramatec and was partially funded by DOE grant DE-FE0000408. Technical discussions with Shekar Balagopal, Dr. Sai Bhavaraju, Tony Elangovan, Marc Flinders, John Gordon, Lyle Miller, Mike Whittaker, Professor Dinesh Shetty, and Professor Anil Virkar were very helpful. Also, I am especially grateful for Tiffany's constant support during the stressful and sometimes difficult times.

1. INTRODUCTION

1.1 Background

Consumer electronics, such as laptop computers and smart phones, drive current interest in and demand for lightweight, low-impedance Li-ion batteries. Liquid electrolyte-based systems with Li inorganic oxides as intercalation compounds [1,2] and polymer membrane separators dominate the commercialized Li-ion technology currently in use. While these systems have enjoyed much success and continue to do so, the possible use of Li-ion batteries in automotive, aerospace, and industrial-scale energy storage applications [3-8] is accompanied by the necessity of overcoming the limited temperature range and safety concerns inherent to organic electrolyte and polymer-based batteries [9-11]. Appealing approaches that have seen a significant research effort include the use of solid electrolytes in all solid-state batteries and as positive and/or negative electrodes in an aqueous electrolyte alternative to the current battery configuration [12-20]. Li et al. [21] introduced the first aqueous rechargeable Li-ion battery in 1994 which would have a clear advantage over their nonaqueous counterparts in terms of being safer, cheaper, and more environmentally friendly [17,22-25].

Lithium titanium phosphate (LTP) is a Li-ion conducting material from the sodium zirconium phosphate (NZP) family being considered as a negative electrode material in aqueous Li-ion batteries [12,26-30]. Hagman and Kierkegaard [31] reported fast transport of Na^+ ions through the NZP structure, $NaZr_2(PO_4)_3$. Hong et al. [32,33]

and Goodenough et al. [34,35] pioneered the NZP family as fast ion conductors, realizing that Li^+ could be substituted for Na^+ in the structure. It is not only possible to replace Na^+ by Li^+, but Ti^{4+} substitution for Zr^{4+} results in LTP ($LiTi_2(PO_4)_3$) materials. Further substitution of Al^{3+} at the Ti^{4+} site results in LATP with formula $Li_{1.3}Al_{0.3}Ti_{1.7}(PO_4)_3$, increasing the Li^+ concentration for charge neutrality [36]. LTP has an open-circuit potential of 2.5 V with respect to Li metal, which is below the 2.6 V decomposition potential of aqueous electrolytes at standard temperature and pressure [15] and has good electrochemical stability in water over a pH range of 7–9 [12,30], making it an ideal candidate for use in aqueous Li-ion batteries.

However, LTP has significantly lower conductivity than the Al-doped LATP first reported by Aono et al. [36]. LATP possesses adequate ionic conductivity in an aqueous electrochemical cell to be used in many electrochemical applications, including as an electrode material in aqueous Li-ion batteries and as a Li transporting separator for aqueous stream purification and concentration [37-39]. However, it has often been reported in the literature that LATP is not water stable, and although stability has been enhanced with slight additions of Si at the P site according to $Li_{1+x+y}Al_xTi_{2-x}Si_yP_{3-y}O_{12}$, where x is ~0.25 and y is 0.1 – 0.3 [40-42], these materials still exhibited poor stability in water and degraded in alkaline solutions, namely LiOH, after even short exposure times [43-45].

Another difficulty with materials from the NZP family is well-documented high thermal expansion anisotropy between the a and c lattice parameters [46]. If grains exceed a critical size in polycrystalline materials, microcracking along grain boundaries occurs due to the difference in contraction upon cooling from the sintering temperature.

Cleveland and Bradt [47,48] showed that critical grain size for microcracking, $GS_{critical}$, could be calculated as

$$GS_{critical} = \frac{14.4\gamma_f}{E(\Delta\alpha_{max})^2(\Delta T)^2} \quad (1.1)$$

where γ_f is the fracture surface energy for grain boundary microcracking, $\Delta\alpha_{max}$ is the difference between the maximum and minimum principal axial thermal expansion coefficients of the unit cell, ΔT is the temperature differential to initiate microcracking during cooling, and E is Young's modulus. Bradt [48] showed that the critical grain size for NZP materials ranged between 2 and 13 μm. The higher anisotropy of LTP materials [49,50] suggests that the critical grain size for LATP may be below 2 μm. Thus, grains in the sintered ceramic must be kept small to maintain strength and avoid discontinuity in a dense microstructure.

Ultimately, if long-term stability of LATP could be demonstrated under electrochemical conditions in aqueous media, especially in inexpensive solutions such as LiOH, it could lead to several applications, including aqueous Li-ion batteries. In many studies, LATP has been determined to be stable or unstable in a given media due solely to changes in XRD patterns and/or a.c. impedance spectra. Also, since microcracking may play a role in the feasibility of using an LATP material in an electrochemical cell, it must be investigated to determine its effect on conductivity and membrane strength. The objectives of this thesis were to: 1) show evidence that microcracking can lower the ionic conductivity of LATP materials; 2) compare the d.c. conductivity of LATP in various Li salts, at the same Li^+ content, in aqueous solutions tested at 40°C; 3) use

strength measurements on ceramic membranes as a means of monitoring electrochemical degradation; and 4) identify parameters which allow LATP to be used in aqueous environments. Objective 1 is covered in Chapter 2 [37], objectives 2-4 are addressed in Chapter 3 [51], and Chapter 4 provides a summary and conclusions.

1.2 References

1. M.S. Whittingham, "Electrical Energy Storage and Intercalation Chemistry," *Science* **192** (1976) 1126-1127.

2. B.C.H. Steele, "Fast Ion Transport in Solids: Solid-State Batteries and Devices," North-Holland/American Elsevier, Inc., Amsterdam-London/New York, (1973).

3. A.D. Pasquier, I. Plitz, S. Menocal, and G. Amatucci, "A Comparative Study of Li-Ion Battery, Supercapacitor, and Nonaqueous Asymmetric Hybrid Devices for Automotive Applications," *J. Power Sources* **115** (2003) 171-178.

4. K.T. Chau, Y.S. Wong, and C.C. Chan, "An Overview of Energy Sources for Electric Vehicles," *Energy Conver. Manage.* **40** (1999) 1021-1039.

5. P.C. Frost, "Developments in Lead-acid Batteries: A Lead Producer's Perspective," *J. Power Sources* **78** (1999) 256-266.

6. P. Gifford, J. Adams, D. Corrigan, and S. Venkatesan, "Development of Advanced Nickel/Metal Hydride Batteries for Electric and Hybrid Vehicles," *J. Power Sources* **80** (1999) 157-163.

7. D.H. Doughty, P.C. Butler, A.A. Akhil, N.H. Clark, and J.D. Boyes, "Batteries for Large-scale Stationary Electrical Energy Storage," *J. Electrochem. Soc. Interface* (2010) 49-53.

8. T. Tanaka, K. Ohta, and N. Arai, "Year 2000 R&D Status of Large-scale Lithium Ion Secondary Batteries in the National Project of Japan," *J. Power Sources* **97-98** (2001) 2-6.

9. J.W. Fergus, "Ceramic and Polymeric Solid Electrolytes for Lithium-ion Batteries," *J. Power Sources* **195** (2010) 4554-4569.

10. P. Knauth, "Inorganic Solid Li-Ion Conductors: An Overview," *Solid State Ionics* **180** (2009) 911-916.

11. N. Anantharamulu, K.K. Rao, G. Rambabu, B.V. Kumar, V. Radha, and M. Vithal, "A Wide-ranging Review on Nasicon Type Materials," *J. Mater. Sci.* **46** (2011) 2821-2837.

12. J.Y. Luo, W.J. Cui, P. He, and Y.Y. Xia, "Raising the Cycling Stability of Aqueous Lithium-ion Batteries by Eliminating Oxygen in the Electrolyte," *Nat. Chem.* **2** (2010) 760-765.

13. C.M. Burba and R. Frech, "Vibrational Spectroscopic Study of Lithium Intercalation into $LiTi_2(PO_4)_3$," *Solid State Ionics* **177** (2006) 1489-1494.

14. A.K. Padhi, K.S. Nanjundaswamy, and J.B. Goodenough, "Phospho-olivines as Positive-Electrode Materials for Rechargeable Lithium Batteries," *J. Electrochem. Soc.* **144** (1997) 1188-1194.

15. C. Delmas, A. Nadiri, and J.L. Soubeyroux, "The Nasicon-type Titanium Phosphates $ATi_2(PO_4)_3$ (A=Li, Na) as Electrode Materials," *Solid State Ionics* **28** (1988) 419-423.

16. G. Wang, L. Fu, N. Zhao, L. Yang, Y. Wu, and H. Wu, "An Aqueous Rechargeable Lithium Battery with Good Cycling Performance," *Angew. Chem. Int. Ed.* **46** (2007) 295-297.

17. J. Kohler, H. Makihara, H. Uegaito, H. Inoue, and M. Toki, "LiV_3O_8: Characterization as Anode Material for an Aqueous Rechargeable Li-Ion Battery System," *Electrochim. Acta* **46** (2000) 59-65.

18. Y.G.Wang and Y.Y. Xia, "A New Concept Hybrid Electrochemical Supercapacitor: Carbon/$LiMn_2O_4$ Aqueous System," *Electrochem. Commun.* **7** (2005) 1138-1142.

19. G.X.Wang, S. Zhong, D.H. Bradhurst, S.X. Dou, and H.K. Liu, "Secondary Aqueous Lithium-ion Batteries with Spinel Anodes and Cathodes," *J. Power Source*s **74** (1998) 198-201.

20. N.C. Li, C.J. Patrissi, G.L. Che, and C.R. Martin, "Rate Capabilities of Nanostructured $LiMn_2O_4$ Electrodes in Aqueous Electrolyte," *J. Electrochem. Soc.* **147** (2000) 2044-2049.

21. W. Li, J.R. Dahn, and D.S. Wainwright, "Rechargeable Lithium Batteries with Aqueous Electrolytes," *Science* **264** (1994) 1115-1118.

22. W. Li and J.R. Dahn, "Lithium-Ion Cells with Aqueous Electrolytes," *J. Electrochem. Soc.* **142** (1995) 1742-1746.

23. H.Q. Yang, D.P. Li, S. Han, N. Li, and B.X. Lin, "Vanadium-manganese Complex Oxides as Cathode Materials for Aqueous Solution Secondary Batteries," *J. Power Sources* **58** (1996) 221-224.

24. A. Eftekhari, "Electrochemical Behavior of Thin-film $LiMn_2O_4$ Electrode in Aqueous Media," *Electrochim. Acta* **47** (2001) 495-499.

25. J.W. Lee and S.I. Pyun, "Investigation of Lithium Transport Through $LiMn_2O_4$ Film Electrode in Aqueous $LiNO_3$ Solution," *Electrochim. Acta* **49** (2004) 753-761.

26. X.H. Liu, T. Saito, T. Doi, S. Okada, and J. Yamaki, "Electrochemical Properties of Rechargeable Aqueous Lithium Ion Batteries with an Olivine-type Cathode and a Nasicon-type Anode," *J. Power Sources* **189** (2009) 706-710.

27. N.V. Kosova, D.I. Osintsev, N.F. Uvarov, and E.T. Devyatkina, "Lithium Titanium Phosphate as Cathode, Anode, and Electrolyte for Lithium Rechargeable Batteries," *Chem. Sustain. Dev.* **13** (2005) 253-260.

28. J.Y. Luo and Y.Y. Xia, "Aqueous Lithium-ion Battery $LiTi_2(PO_4)_3/LiMn_2O_4$ with High Power and Energy Densities as well as Superior Cycling Stability," *Adv. Funct. Mater.* **17** (2007) 3877-3884.

29. H. Wang, K. Huang, Y. Zeng, S. Yang, and L. Chen, "Electrochemical Properties of TiP_2O_7 and $LiTi_2(PO_4)_3$ as Anode Material for Lithium Ion Battery with Aqueous Solution Electrolyte," *Electrochim. Acta* **52** (2007) 3280-3285.

30. R.B. Shivashankaraiah, H. Manjunatha, K.C. Mahesh, G.S. Suresh, and T.V. Venkatesha, "Electrochemical Characterization of $LiTi_2(PO_4)_3$ as Anode Material for Aqueous Rechargeable Lithium Batteries," *J. Electrochem. Soc.* **159** (2012) A1074-A1082.

31. L. Hagman and P. Kierkegaard, "The Crystal Structure of $NaMe_2^{IV}(PO_4)_3$; Me^{IV}=Ge, Ti, Zr," *Acta Chem. Scand.* **22** (1968) 1822-1832.

32. H.Y.P. Hong, "Crystal Structure and Crystal Chemistry in the System $Na_{1+x}Zr_2Si_xP_{3-x}O_{12}$," *Mater. Res. Bull.* **11** (1976) 173-182.

33. H.YP. Hong, J.A. Kafalas, and M. Bayard, "High Na^+-ion Conductivity in $Na_5YSi_4O_{12}$," *Mater. Res. Bull.* **13** (1978) 757-761.

34. J.B. Goodenough, H.Y.P. Hong, and J.A. Kafalas, "Fast Na^+-ion Transport in Skeleton Structures," *Mater. Res. Bull.* **11** (1976) 203-220.

35. J.B. Goodenough, "NASICON I Structure and Conductivity," *Solid State Ionics* **9/10** (1983) 793-794.

36. H. Aono, E. Sugimoto, Y. Sadaoka, N. Imanaka, and G. Adachi, "Ionic Conductivity of the Lithium Titanium Phosphate ($Li_{1+x}M_xTi_{2-x}(PO_4)_3$, M=Al, Sc, Y, and La) Systems," *J. Electrochem. Soc.* **136** (1989) 590-591.

37. S.D. Jackman and R.A. Cutler, "Effect of Microcracking on Ionic Conductivity in LATP," *J. Power Sources* **218** (2012) 65-72.

38. A.V. Joshi, S. Balagopal, and J. Pendelton, "Electrolytic Method to Make Alkali Alcoholates Using Ion Conducting Alkali Electrolyte/Separator," U.S. Patent 8,075,758 (2011).

39. J.H. Gordon and S. Bhavaraju, "Device and Method for Recovery or Extraction of Lithium," U.S. Patent Application 20120103826 (2012).

40. M. Cretin, P. Fabry, and L. Abello, "Study of $Li_{1+x}Al_xTi_{2-x}(PO_4)_3$ for Li^+ Potentiometric Sensors," *J. Eur. Ceram. Soc.* **15** (1995) 1149-1156.

41. N. Imanishi, S. Hasegawa, T. Zhang, A. Hirano, Y. Takeda, and O. Yamamoto, "Lithium Anode for Lithium-air Secondary Batteries," *J. Power Sources* **185** (2008) 1392-1397.

42. T. Zhang, N. Imanishi, Y. Shimonishi, A. Hirano, Y. Takeda, O. Yamamoto, and N. Sammes, "A Novel High Energy Density Rechargeable Lithium/Air Battery," *Chem. Commun.* **46** (2010) 1661-1663.

43. S. Hasegawa, N. Imanishi, T. Zhang, J. Xie, A. Hirano, Y. Takeda, and O. Yamamoto, "Study on Lithium/Air Secondary Batteries–Stability of NASICON-type Lithium Ion Conducting Glass-ceramics with Water," *J. Power Sources* **189** (2009) 371-377.

44. T. Zhang, N. Imanishi, Y. Shimonishi, A. Hirano, J. Xie, Y. Takeda, O. Yamamoto, and N. Sammes, "Stability of a Water-Stable Lithium Metal Anode for a Lithium-Air Battery with Acetic Acid-Water Solutions," *J. Electrochem. Soc.* **157** (2010) A214-A218.

45. Y. Shimonishi, T. Zhang, N. Imanishi, D. Im, D.J. Lee, A. Hirano, Y. Takeda, O. Yamamoto, and N. Sammes, "A Study on Lithium/Air Secondary Batteries–Stability of NASICON-type Lithium Ion Conducting Solid Electrolyte in Alkaline Aqueous Solutions," *J. Power Sources* **196** (2011) 5128-5132.

46. T. Oota and I. Yamai, "Thermal Expansion Behavior of NaZr2(PO4)3 Type Compounds," *J. Am. Ceram. Soc.* **69** (1986) 1-6.

47. J. J. Cleveland and R.C. Bradt, "Grain Size/Microcracking Relations for Pseudobrookite Oxides," *J . Am. Ceram. Soc.* **61** (1978) 478-481.

48. R.C. Bradt, "The Critical Grain Size for Microcracking in Low Thermal Expansion Anisotropic Ceramics," *Ceram. Trans.* **52** (1995) 5-18.

49. C.Y. Huang, D.K. Agrawal, and H.A. McKinstry, "Thermal Expansion Behavior of $M'Ti_2P_3O_{12}$ (M'=Li, Na, K, Cs) and $M''Ti_4P_6O_{24}$ (M''=Mg, Ca, Sr, Ba) Compounds," *J. Mater. Sci.* **30** (1995) 3509-3514.

50. D.A. Woodcock and P. Lightfoot, "Comparison of the Structure Behavior of the Low Thermal Expansion NZP Phases $MTi_2(PO_4)_3$ (M=Li, Na, K)," *J. Mater. Chem.* **9** (1999) 2907-2911.

51. S.D. Jackman and R.A. Cutler, "Stability of Nasicon-type $Li_{1.3}Al_{0.3}Ti_{1.7}P_3O_{12}$ in Aqueous Solutions," *J. Power Sources* manuscript # POWER-D-12-02684 (2012).

2. EFFECT OF MICROCRACKING ON IONIC CONDUCTIVITY OF LATP

2.1 Abstract

Because of high thermal expansion anisotropy, lithium aluminum titanium phosphate (LATP) is prone to microcrack generation like other sodium zirconium phosphate (NZP) type materials. While much attention has been given to the role of grain boundary phases on the ionic conductivity of LATP, microcracking is also expected to lower conductivity.

While all LATP materials characterized had grains larger than the critical size for microcracking, fine-grained (1.7±0.7 μm) LATP had twice the ionic conductivity of the same purity of coarse-grained (4.8±1.9 μm) LATP at 323 K due to less extensive cracking at grain boundaries. While the increases in Young's modulus (81 GPa to 115 GPa) and biaxial strength (26±2 MPa to 123±17 MPa) are consistent with the reduction in grain size, the increase in conductivity is a strong driving force for avoiding large LATP grains. Lower purity degraded ionic conductivity for similar grain sizes, as expected.

Single-edged precracked beam fracture toughness measurements showed that the fine-grained, high-purity LATP has a K_{Ic} value of 1.1±0.3 MPa$\sqrt{m}$. Flexural strength measurements (147±14 MPa) indicated that the critical flaw size was on the order of 30

μm, with processing flaws still limiting strength. It is expected that as grain size is further reduced, strength and ionic conductivity will continue to improve in tandem until microcracking is eliminated, whereupon any further decrease in grain size should increase grain boundary resistivity and decrease overall ionic conductivity.

2.2 Introduction

Consumer electronics, such as laptop computers and smart phones, drive current interest in and demand for lightweight, low-impedance Li-ion batteries. Liquid electrolyte-based systems with Li inorganic oxides as intercalation compounds [1,2] and polymer membrane separators dominate the commercialized Li-ion technology currently in use. While these systems have enjoyed much success and continue to do so, the possible use of Li-ion batteries in larger scale automotive and aerospace applications is accompanied by the necessity of higher capacity and energy storage with less loss of charge when not in use. Solid electrolytes with high potential and capacity could find use in such applications.

Hagman and Kierkegaard [3] reported fast transport of Na^+ ions through the sodium zirconium phosphate (NZP) structure ($NaZr_2(PO_4)_3$). Hong et al. [4,5] and Goodenough et al. [6,7] pioneered the NZP family as fast ion conductors, realizing that Li^+ could be substituted for Na^+ in the structure. It is not only possible to replace Na^+ by Li^+, but Ti^{4+} substitution for Zr^{4+} results in LTP ($LiTi_2(PO_4)_3$) materials, which are called by the acronym LATP when Al^{3+} is incorporated into the structure, increasing the Li^+ concentration for charge neutrality [8]. The major advantage of LATP is high ionic conductivity near room temperature [9].

High thermal expansion anisotropy between the *a* and *c* lattice parameters is well-documented in the NZP family of materials [10]. If grains exceed a critical size in polycrystalline materials, microcracking along grain boundaries occurs due to the difference in contraction upon cooling from the sintering temperature. Cleveland and Bradt [11,12] showed that critical grain size for microcracking, $GS_{critical}$, could be calculated as

$$GS_{critical} = \frac{14.4\gamma_f}{E(\Delta\alpha_{max})^2(\Delta T)^2} \quad (2.1)$$

where γ_f is the fracture surface energy for grain boundary microcracking, $\Delta\alpha_{max}$ is the difference between the maximum and minimum principal axial thermal expansion coefficients of the unit cell, ΔT is the temperature differential to initiate microcracking during cooling, and E is Young's modulus. Bradt [12] showed that the critical grain size for NZP materials ranged between 2 and 13 μm. The higher anisotropy of LTP materials [13,14] suggests that the critical grain size for LATP may be below 2 μm.

Although the NZP structure is highly disordered, it exhibits open channels between ion sites, giving LATP materials relatively high ionic conduction through the lattice (bulk) of 10^{-3} S cm^{-1} even at ambient temperature [8]. Impurities often segregate to grain boundaries and lower conductivity in ionic conductors. Coarser grained materials have fewer grain boundaries; therefore, as grain size decreases the grain boundary influence on conductivity increases, lowering the total conductivity [15]. In general, as grains become coarser, the bulk conductivity component of total ionic conductivity begins to dominate. In microcracked materials, however, one might expect

that ionic conductivity would increase as grain size decreases, since microcracks will impede ionic conductivity.

The Hall-Petch relationship, which is often used to explain the effect of grain size on strength for metals, suggests that the strength of a material should increase with the inverse square root of grain size. Metals are strengthened by dislocation motion so that grains act as barriers for dislocation movement, increasing strength. In ceramics, dislocation mobility is low at ambient temperatures, so grain size is only a way to increase strength if it acts as the critical flaw or is linked to the critical flaw size. For many polycrystalline ceramics, processing allows the grain size to influence the critical flaw size such that strength increases as the grain size decreases [16]. A better predictor of strength is the critical flaw size, c, which is related to fracture strength, σ_f, as

$$K_{Ic} = Y\sigma_f\sqrt{c} \tag{2.2}$$

where K_{Ic} is the fracture toughness and Y is a geometrical factor dependent on both crack size and shape. The fracture toughness of LATP is expected to be low, since NZP has a fracture toughness of 1.0±0.2 MPa√m [17]. Strength is expected to be related to the inverse square root of the critical flaw size, which may be a pore, network of microcracks, agglomeration of grains, or other defects introduced during processing.

The purpose of this paper is to show evidence that microcracking can lower the ionic conductivity of LATP materials, as well as determine the fracture toughness of fine-grained LATP so that the critical flaw size can be assessed. It was hypothesized that by

lowering grain size, ionic conductivity and strength could be simultaneously increased for high-purity $Li_{1.3}Al_{0.3}Ti_{1.7}(PO_4)_3$.

2.3 Experimental

2.3.1 Phase- Purity and Characterization of Physical and Mechanical Properties

All testing was performed on sintered LATP specimens that were obtained from Ceramatec, Inc. (Salt Lake City, Utah). Four experimental grades were prepared using proprietary processing. These specimens were characterized using an X-ray diffractometer (Philips PW3040) to verify the LATP phase and identify any secondary phases. Scans were conducted with Cu K_α radiation over a 2θ range of 15-75° using a step size of 0.02° and a 0.05 s dwell time. Rietveld refinement was used to quantify the amount of additional phases when present [18]. LATP specimens were categorized as either low-purity, fine-grained (LPFG), moderate-purity, fine-grained (MPFG), high-purity, coarse-grained (HPCG), or high-purity, fine-grained (HPFG) specimens based on experimental findings. LPFG and MPFG specimens were specimens with distinct secondary phases while HPCG and HPFG specimens were phase-pure by X-ray diffraction (XRD) with coarse-grained and fine-grained microstructures, respectively.

Density based on Archimedes' principle was measured in water, from which the percentage of open porosity could also be calculated. The microstructure of those specimens used for strength and conductivity testing was examined using a scanning electron microscope (JEOL JSM-5900LV SEM) and a microhardness tester (LECO LM-100). Fracture surfaces of specimens broken during biaxial strength testing as well as

surfaces polished with an automatic polisher (LECO Spectrum System 2000) were examined.

The biaxial strength of compositions with varying grain sizes and both phase-pure LATP and batches showing secondary phases were determined using a universal testing machine (Instron model 5566) with a 1 kN load cell using a ring-on-ring test (ASTM C1499-04). The support ring had a radius on the compressive side of 6.5 mm and a radius on the tension side of 9.5 mm. A thin piece of adhesive was placed on the compressive side to keep the broken disk pieces together. A steel ball was held with the top ring fixture through lowering until contact was made with the ceramic. Cross-head displacement was 0.5 mm min^{-1}, and data were collected every 50 ms. The biaxial fracture strength, σ_b, was calculated using [19]

$$\sigma_b = \frac{3P}{2\pi t^2}\left[(1-\nu)\frac{D_S - D_L}{2D^2} + (1+\nu)ln\left(\frac{D_S}{D_L}\right)\right] \quad (2.3)$$

where P is the applied load, t is the specimen thickness, ν is Poisson's ratio, D_S and D_L are the support and load ring diameters, respectively, and D is the specimen diameter. Biaxial strength measurements were important to shed light on the properties specific to LATP in the form of a thin, flat membrane. A Weibull probability function [20] is often used to characterize the reliability of brittle materials as

$$ln\left(ln\left(\frac{1}{1-F}\right)\right) = mln(\sigma_b) - mln(\sigma_0) \quad (2.4)$$

where F is the probability of failure, m is the Weibull modulus, and σ_0 is the characteristic strength. The Weibull modulus indicates the variability in measured strength, with a higher modulus correlating to greater consistency in strength. The characteristic stress is found when σ_f is equal to σ_0, leading to an F of 0.632, meaning there is a probability that 63.2% of specimens would fail at this calculated stress.

Flexural strength on bars of nominal dimensions 3 mm x 4 mm x 45 mm tested at a loading rate of 0.5 mm min^{-1} was calculated as [21]

$$\sigma_f = \frac{1.5PS}{wt^2} \tag{2.5}$$

where S is the difference between the inner and outer spans of the fixture (20 mm), w is the specimen width, and t is the thickness.

Young's modulus measurements were taken at low strains on coarse- and fine-gained specimens by using a strain gauge adhered to the test section of the specimen to determine the loading/unloading trends.

The single-edge precracked beam (SEPB) method (ASTM C1421-10) was used to measure fracture toughness. Bars were first indented with a diamond Knoop indenter at 98 N, and then precracked (Maruto model MBK-603C Precracker) with a 6 mm span. The fracture toughness was calculated as [22]

$$K_{Ic} = \frac{P(S_o - S_i)}{tw^{1.5}}\left(\frac{3\left(\frac{a}{w}\right)^{1.5}}{2\left(1-\frac{a}{w}\right)^{1.5}}\right)\left[1.9887 - 1.326\left(\frac{a}{w}\right) - \left(\frac{\left\{3.49-0.68\left(\frac{a}{w}\right)+1.35\left(\frac{a}{w}\right)^2\right\}\left[\frac{a}{w}\right]\left\{1-\left(\frac{a}{w}\right)\right\}}{\left(1+\left(\frac{a}{w}\right)\right)^2}\right)\right] \tag{2.6}$$

where S_o and S_i are the outer and inner spans, respectively, and a is the crack length. The value of a/w was measured by analyzing the fracture surface with a stereomicroscope (Nikon SMZ1000) after the specimens had been tested.

Bars with nominal dimensions 5 mm x 5 mm x 15 mm were thermally cycled 3 times in a dilatometer (Unitherm Model 1161) between T = 25°C and 600°C with a heating and cooling rate of 2°C min^{-1} to measure thermal expansion.

2.3.2 Ionic Conductivity Measurements

Pellets with a 15 mm diameter and 5 mm thickness were used for a.c. impedance measurements to provide enough resistance to ion transport at elevated temperatures that grain boundary arcs remained discernible from bulk arcs. Gold electrodes were sputtered onto both sides of the pellet with a sputter coater (Fullam EffaCoater). Five consecutive impedance measurements were taken at each temperature, ranging from ambient to 150°C in 25°C increments. Measurements were made with a spectrometer (Solartron SI 1260 Impedance/Gain-Phase) at an a.c. amplitude of 40 mV over a frequency range of 500 Hz to 10 MHz. The activation energy was obtained by plotting the logarithm of ionic conductivity times temperature as a function of inverse temperature based on the expected Arrhenius behavior.

For d.c. conductivity measurements, 25 mm diameter by 1 mm thick disks were used with Ni electrodes. Tests were conducted at T = 50°C with a current density of 25 mA cm^{-2} in aqueous 7 wt% LiOH. Commercial software (*Labview*) was used to collect the voltage and current readings at 1 min intervals throughout the duration of the test. The voltage due to reactions at the electrodes was measured in situ without a membrane in the cell separating the cathode and anode compartments to obtain a 'blank' reading.

This was used to calculate the resistance due solely to the membrane for d.c. conductivity calculations.

2.4 Results and Discussion

2.4.1 Phase-Purity, Physical and Mechanical Properties

Phase-purity was evaluated by XRD with scans as displayed in Figure 2.1. High-purity specimens were $Li_{1.3}Al_{0.3}Ti_{1.7}(PO_4)_3$ with no secondary phases detectable via XRD analysis. The low-purity specimens showed combinations of $AlPO_4$, TiO_2, and $LiTiPO_5$ phases that have low ionic conductivity and are frequently reported in the literature [23-25]. Rietveld refinement showed that LPFG specimens contained 36.5 wt% $LiTiPO_5$ and 6.5 wt% $AlPO_4$, the expected LATP phase comprising the remainder. MPFG specimens had less pronounced secondary phases, but 1.2 wt% $AlPO_4$ and 4.0 wt% TiO_2 were still detected by Rietveld analysis. Peaks corresponding to these phases are most prominent at 2θ values of 21.8° ($AlPO_4$), 27.4° (TiO_2), 36.1° (TiO_2), and 41.2° (TiO_2). Kumar et al. [26] showed the deleterious effects of secondary phases on ionic conductivity at varying concentrations, sometimes lowering orders of magnitude over a few volume percents and eventually leading to space charge and blocking effects at higher concentrations. While the two high-purity materials may still have secondary phases below the detection limit of XRD, none were seen with either optical or SEM microscopy.

Calculated lattice parameters for both HPFG and HPCG samples are presented against indexed values in Table 2.1. The addition of Al into the lattice has the overall effect of shortening the unit cell dimensions, slightly decreasing the unit cell volume.

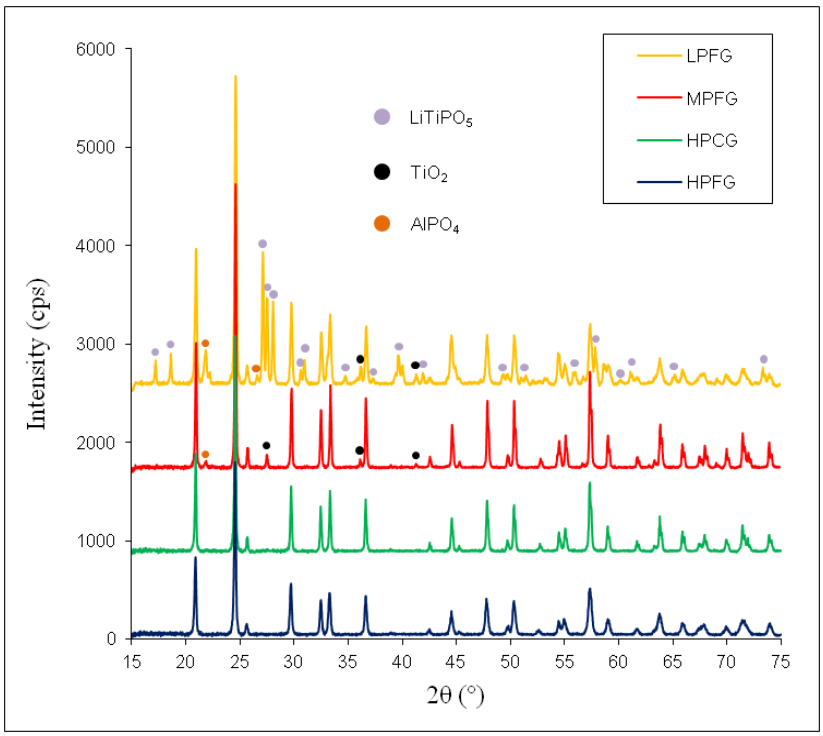

Figure 2.1. XRD scans of LPFG, MPFG, HPCG, and HPFG LATP.

This, however, does not appear to decrease the mobility of Li-ions within the structure to any great extent [3]. Table 2.1 also presents evidence that there is no significant difference in lattice parameters between coarse- and fine-grained materials tested in this study. The theoretical density, ρ_{th}, is easily calculated using the unit cell parameters as

$$\rho_{th} = \frac{Z \cdot MW}{V_c . N_A} \tag{2.7}$$

where Z is the number of molecules per unit cell, MW is molecular weight, V_c is the volume of the unit cell, and N_A is Avogadro's number. Using Equation (2.7), a theoretical density of 2.947 g cm^{-3} was calculated for LATP, assuming a phase-pure material.

Table 2.1

Lattice Parameters and Unit Cell Volumes for LATP

	a (Å)	c (Å)	α (°)	γ (°)	V (Å^3)
HPCG	8.507(1)	20.821(2)	90	120	1305.04
HPFG	8.482(2)	20.804(5)	90	120	1296.36
Indexed Values[a]	8.513	20.878	90	120	1310.31

[a] Values correspond to LTP structure

Figure 2.2 shows a comparison of SEM images taken of as-sintered, fracture, and polished and etched surfaces for LPFG, HPCG, and HPFG specimens. Grain sizes calculated from the SEM images along with density data are summarized in Table 2.2. The images revealed porosity, in accord with expectations, based on density measurements. All materials have large grains which could lead to microcracking. The phase-pure materials had total porosity on the order of 3-5%. The open porosity in the coarse-grained material is evidence of macrocracking, due to the severe anisotropy in the LATP material, since all porosity is typically closed above about 93% of theoretical density.

While LPFG and HPFG specimens had comparable grain sizes, the LPFG image in Figure 2.2(c) shows a more homogeneous grain size distribution. The secondary grain boundary phases present undoubtedly acted as a grain-growth inhibitor, and a more uniform fine-grained microstructure was maintained. HPCG and HPFG specimens both suffered from localized exaggerated grain growth, but HPCG displayed a much more dramatic effect. The large grains were easily observed both in the fractured and backscattered images, but fine grains surrounded these large grains in all images. Ostwald ripening appeared to be the key factor here, the coarse grains growing larger at the expense of the fine grains [27].

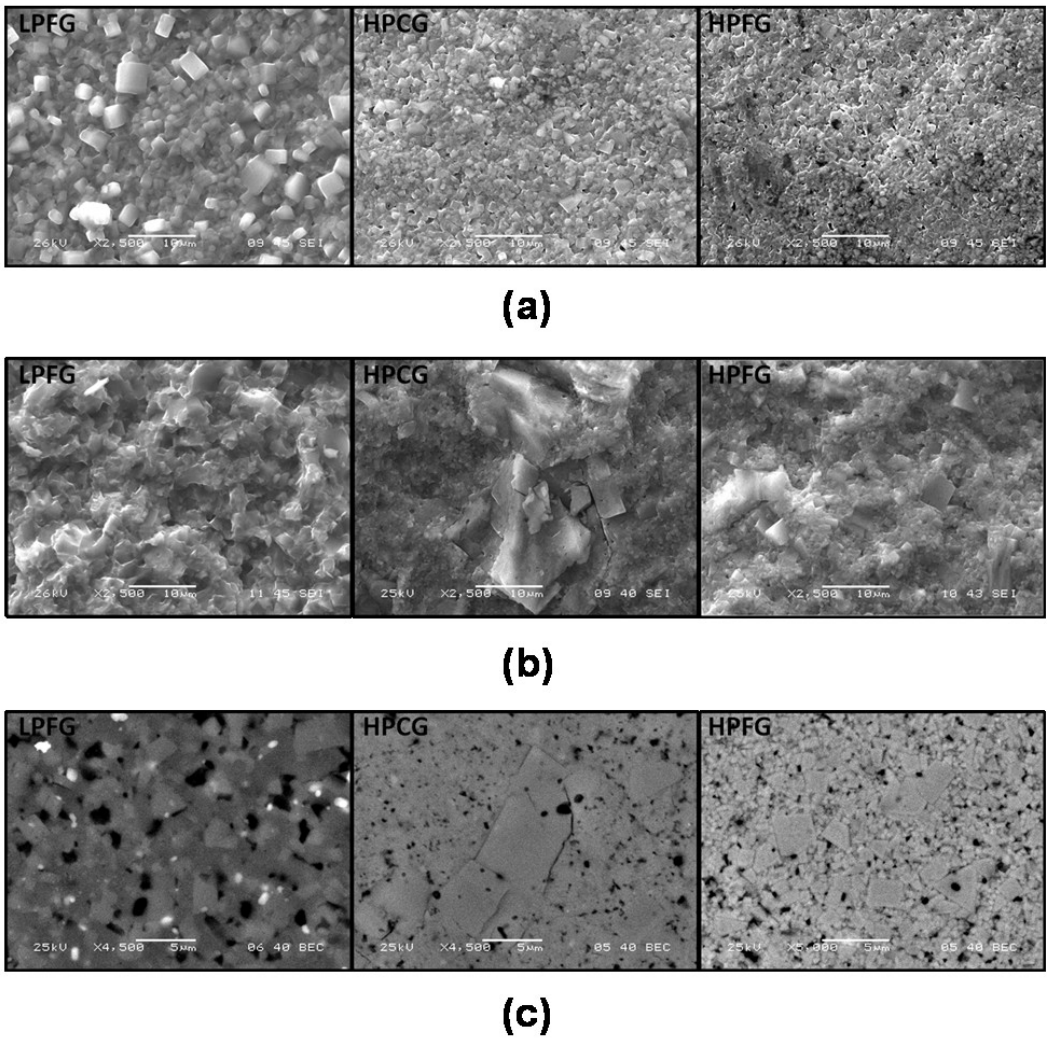

Figure 2.2. SEM images of (a) as-sintered surface, (b) fracture surface, and (c) polished surface of LPFG, HPCG, and HPFG LATP.

Table 2.2

Grain Size and Density of LATP

	Avg. Grain Size (μm)	Largest Grains (μm)	Density (g cm^{-3})	% Open Porosity	% Theoretical Density
LPFG	2.2±0.5	4	2.96	0.2	NA
HPCG	4.8±1.9	30	2.86	1.5	97.0
HPFG	1.7±0.7	9	2.82	0	95.6

Comparisons of fracture surfaces illustrate that all specimens tested appear to have an intergranular mode of failure. Even a crack in a region of localized grain growth in a HPCG specimen seen in Figure 2.3(a) did not appear to result in transgranular fracture, indicating that regardless of grain size, fracture was determined by a grain boundary phenomenon. It is hypothesized that as the grains grow, microcracking dominates fracture behavior. Anisotropy in thermal expansion induces internal stresses that result in extensive microcracking due to high stresses and weak grain boundaries [28]. Figure 2.3(b) provides evidence of this grain boundary macrocracking due to linked microcracks which greatly weaken the specimen and create a blockade for the ionic motion necessary for conductivity.

The average grain sizes of HPCG and HPFG were 4.8±1.9 μm and 1.7±0.7 μm, respectively. Coarser particles used in processing often result in larger flaws than when finer particles are used. The difference in the biaxial strength between these two specimens is over 90 MPa (see Table 2.3), decreasing 79% from HPFG to HPCG specimens, as shown in Figure 2.4. This unusually large drop in strength over a less dramatic increase in grain size indicates there is more than just processing flaws which

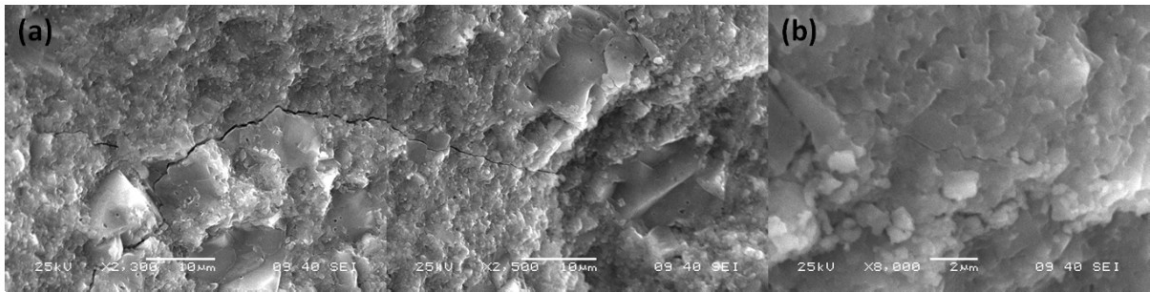

Figure 2.3. SEM micrographs of (a) crack paths and (b) microcracks in HPCG LATP.

Table 2.3

Strength and Young's Modulus of LATP

	Biaxial			Flexural		
	σ_{avg} (MPa)	σ_0 (MPa)	m	σ_{avg} (MPa)	m	E (GPa)
LPFG	49 ± 12	54	5	NA	NA	NA
HPCG	26 ± 2	28	12	NA	NA	81
HPFG	123±17	130	8	147±14	12	115

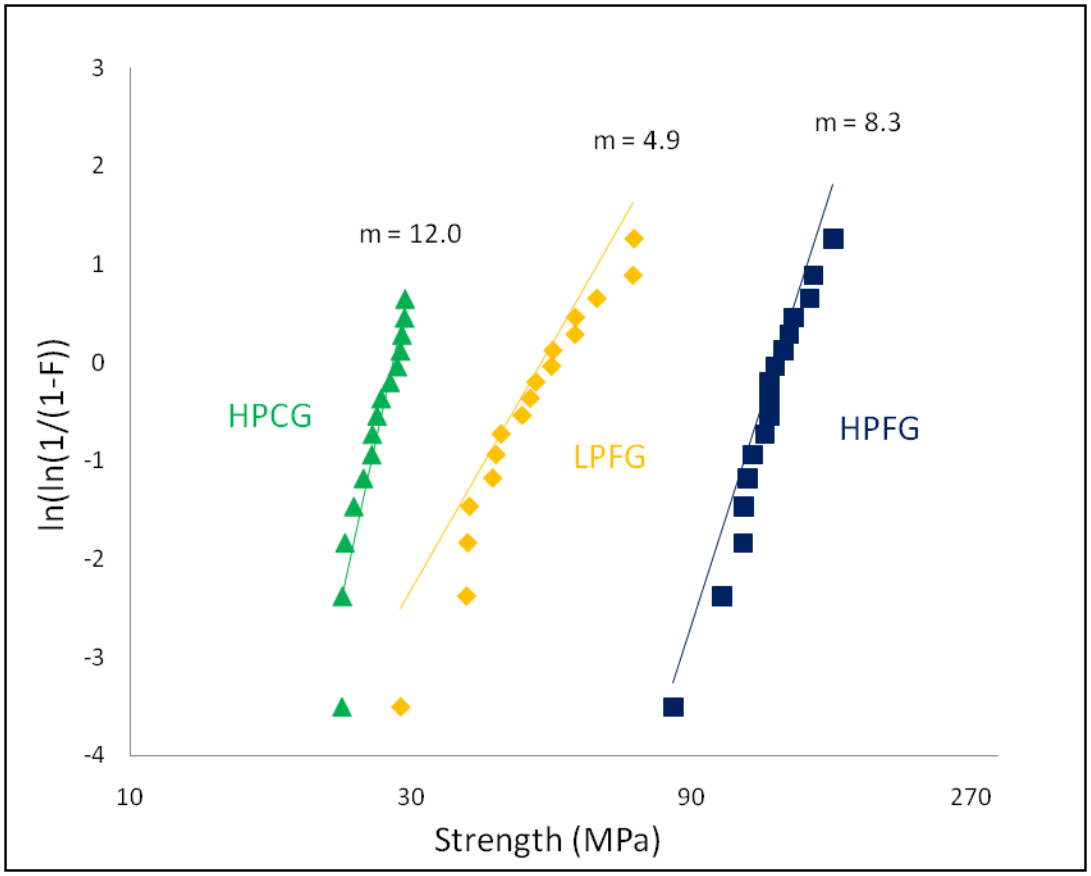

Figure 2.4. Weibull plot of biaxial strength for LPFG, HPCG, and HPFG LATP.

are influenced by grain size affecting the strength of the LATP specimens. A portion of the decreased strength can surely be attributed to larger defects manifest in coarse grains, but the largest contributing factor is believed to be increased microcracking. The low strength in the coarse-grained material is a clear indication of severe microcracking. The higher Weibull modulus calculated for HPCG as compared to HPFG specimens can be explained by its decreased sensitivity to fabrication flaws. The critical flaws necessary to cause fracture at low stresses are inherent to the severely microcracked microstructure, and other flaws resulting from fabrication defects do not exhibit their influence on the mechanical strength.

The strength data and Young's modulus measurements are summarized in Table 2.3. Young's modulus measurements in HPFG over three successive runs showed no difference in measured modulus between runs, but hysteresis in the stress-strain behavior is confirmed in the slightly expanded view of Figure 2.5. The strain behavior of the material as the grains are stretched apart under stress on the tensile side of the bar did not quite match with the behavior of the grains coming back together as this stress is released. This provides further evidence that microcracking exists in even the phase-pure specimens with the most homogeneous grain size measured in this study. The increase in Young's modulus from 81 GPa for HPCG to 115 GPa for HPFG specimens is the effect of decreased microcracking. The Young's modulus value of the extensively microcracked HPCG specimen is in the same range (65-85 GPa) as those previously reported on NZP materials [17,29]. Harshe et al. [30] measured Young's modulus as a function of temperature for a family of NZP materials, showing a maximum value of 105 GPa at high temperature (1100°C) when microcracks had healed. The value of 115 GPa for LATP

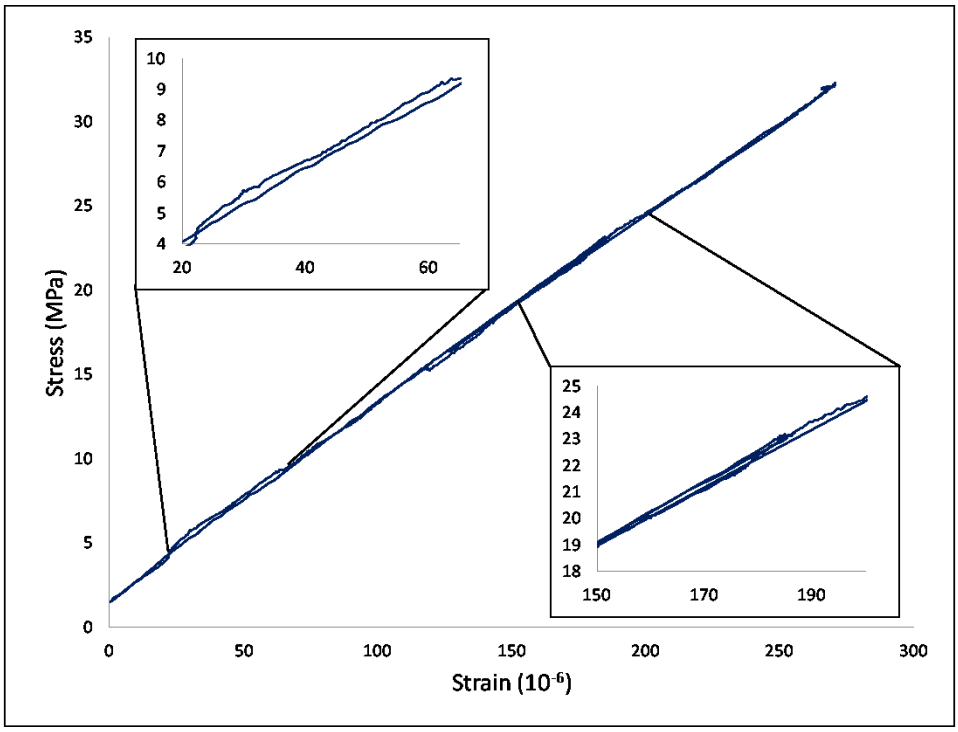

Figure 2.5. Hysteresis in Young's modulus measurement of a HPFG LATP.

appears to be a high modulus for a material from the NZP family. The flexural strength was slightly higher than the biaxial strength, which is not unusual for ceramic materials, where the volume of material under stress controls the strength. The Weibull modulus of 12 is a respectable value for a ceramic material. The fine-grained high-purity material appears to have acceptable strength for a membrane.

Only the fracture toughness of HPFG specimens was tested, the result being 1.1 ± 0.3 MPa√m, a value consistent with a previous measurement on NZP using the same technique [17]. Using Equation (2.2), the fracture toughness allows one to calculate the critical flaw size based on the mean flexural strength. Taking Y=1.29, which is characteristic of surface flaws on flexural specimens, a critical flaw size of 31 μm was calculated for the HPFG LATP. This value is in agreement with the size of flaws identified at fracture origins as shown in Figure 2.6. Higher strength is possible in these

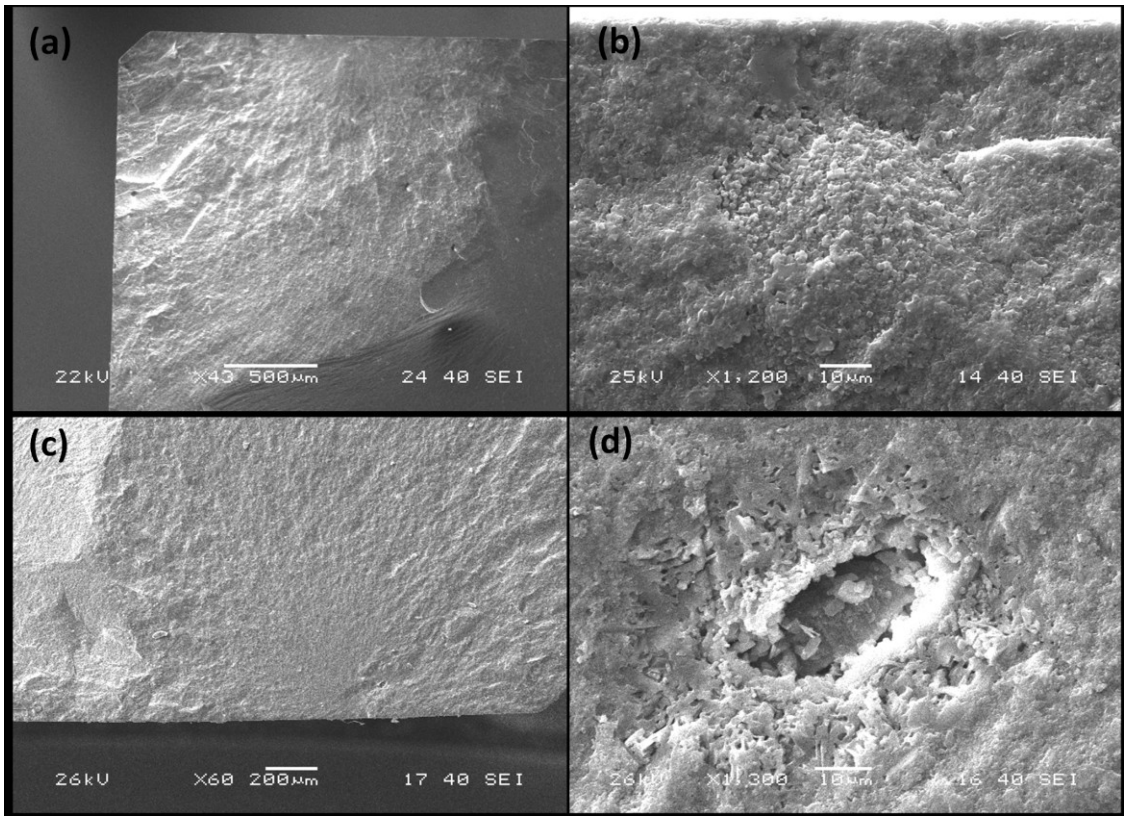

Figure 2.6. SEM micrographs of (a,c) fracture zone and (b,d) higher magnification image of fracture origin in HPFG flexural strength bars.

materials since it is clear that the critical flaw size is due to processing flaws and not large grains, consistent with expectations.

Dilatometer results for HPCG and HPFG specimens are depicted in Figure 2.7. The thermal expansion versus temperature graphs show distinct hysteresis in the path traced upon heating and cooling, although the effect is considerably more pronounced in the HPCG specimen. This suggests that although neither specimen was free from microcracking, the extent was greatly reduced in the HPFG specimen, showing that reduced grain size lessened the tendency to microcrack, as was predicted.

Using Equation (2.1) to estimate the critical grain size for microcracking requires a value of the fracture surface energy for microcracking. Yamai and Oota [31] showed a

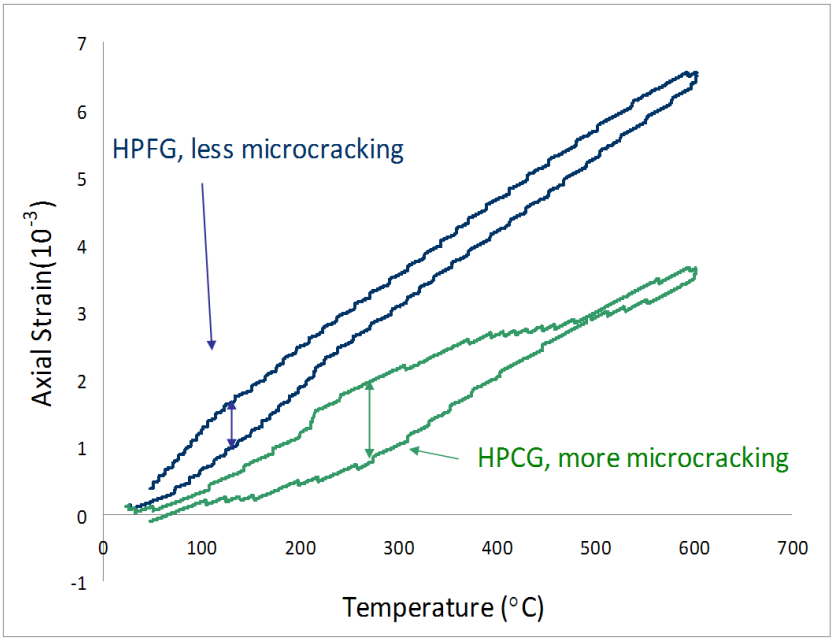

Figure 2.7. Hysteresis in thermal expansion showing microcracking in both HPCG and HPFG LATP.

linear relationship between the critical grain size for microcracking and $(\Delta\alpha_{max})^2$ for a family of NZP materials. Using their data, it is possible to calculate a value of 7 J m^{-2} for γ_f, which is higher than might be expected based on single crystal data [32]. Using thermal expansion data at 800°C given by Woodcock and Lightfoot for LTP for the *a* and *c* crystallographic axes and obtained using variable temperature neutron powder diffraction [14], as well as the Young's modulus value measured in this study, the estimated $GS_{critical}$ of LATP is 1.6 µm. If a more realistic value of 1 J m^{-2} is taken for fracture energy [28], the critical grain size for microcracking decreases to 0.2 µm. Although these calculations are based on thermal expansion data for LTP and not LATP, data collected in this study for HPFG showed a linear thermal expansion of 11.2 x 10^{-6} $°C^{-1}$ at 600°C, which is in good agreement with that reported by Woodcock and Lightfoot of 11.5 x 10^{-6} $°C^{-1}$ [14] for polycrystalline LTP. The trend that anisotropy increases with decreasing cation size shown by Huang [13] holds, making Li-ion-based systems among

the most susceptible to microcracking. This being the case, the microstructure images presented in this study give clear evidence that each tested specimen from all categories was surely microcracked to some extent.

The measured linear thermal expansion of the more severely microcracked HPCG (7.3×10^{-6} °C^{-1}) is significantly lower than HPFG (11.2×10^{-6} °C^{-1}). Since both specimens were confirmed to be of identical phase and composition, this discrepancy can be attributed to the increased presence of microcracked boundaries in HPCG, providing space for internal expansion to occur in cracked grain boundaries before causing bulk expansion [33].

2.4.2 Ionic Conductivity

The most important characteristic of any solid electrolyte is its ability to conduct and transport ions. To some extent, no gain in mechanical properties can adequately compensate for a loss in ionic conductivity. Therefore, it is critical to ensure that the advantageous reduction in microcracks and improvements in strength and toughness correlate with maintaining and/or improving conductivity.

Figure 2.8 gives the Nyquist plots of imaginary impedance versus real impedance for MPFG, HPCG, and HPFG materials. The difference in impedance at the grain boundary for each specimen can clearly be seen by the difference in size of the main semicircle (taken as the grain boundary arc based on capacitance) that eventually turns into a characteristic blocking electrode tail at low frequencies. The difference between high-purity samples is related to the microstructure, not the grain boundary chemistry.

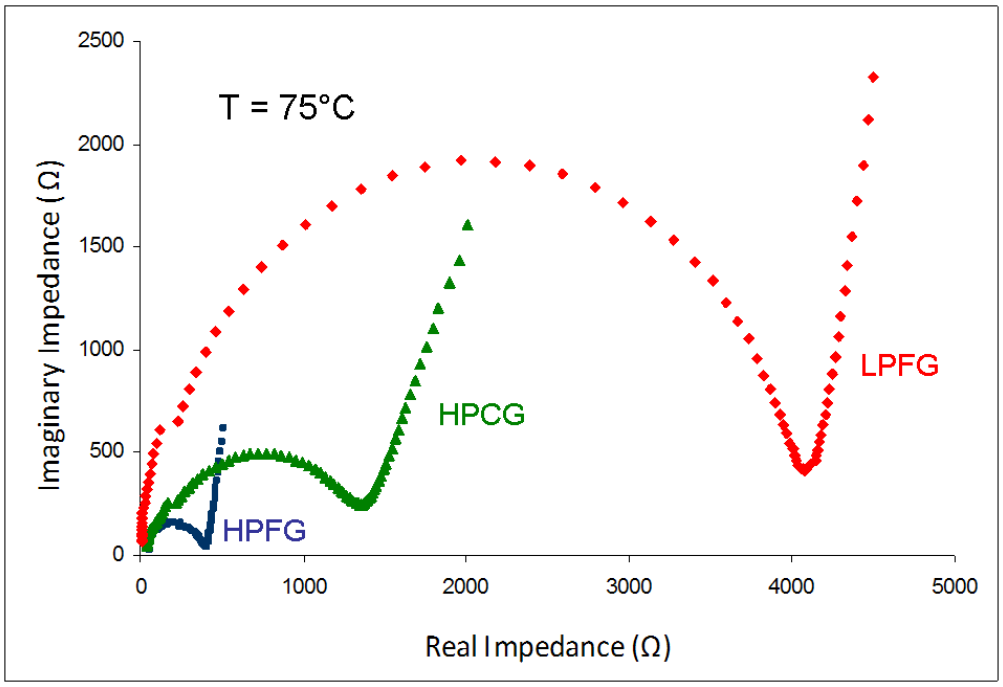

Figure 2.8. Nyquist plots of imaginary versus real impedance for MPFG, HPCG, and HPFG LATP.

The limitations of the impedance spectrometer at frequencies above 10 MHz made full resolution of the bulk arc difficult, but it can be seen that all three semicircles converge to nearly the same nonzero value on the real impedance axis. The high-frequency intercept of each trace was taken to be the bulk resistance for each specimen.

Figure 2.9 is the Arrhenius plot of ionic conductivity and corresponding activation energies for tested specimens. The negative effects of high-impedance secondary phases (MPFG) and a decreased ability for ions to move at the grain boundaries due to microcracking (HPCG) are depicted. Conductivity data (bulk, grain boundary, and total) at all temperatures evaluated are given in Table 2.4. HPFG specimens had the highest conductivity at all temperatures, measuring 0.67 mS cm^{-1} at room temperature, despite having a finer microstructure than HPCG. This counterintuitive trend of increasing grain boundary ionic conductivity with decreasing grain size is another indication of

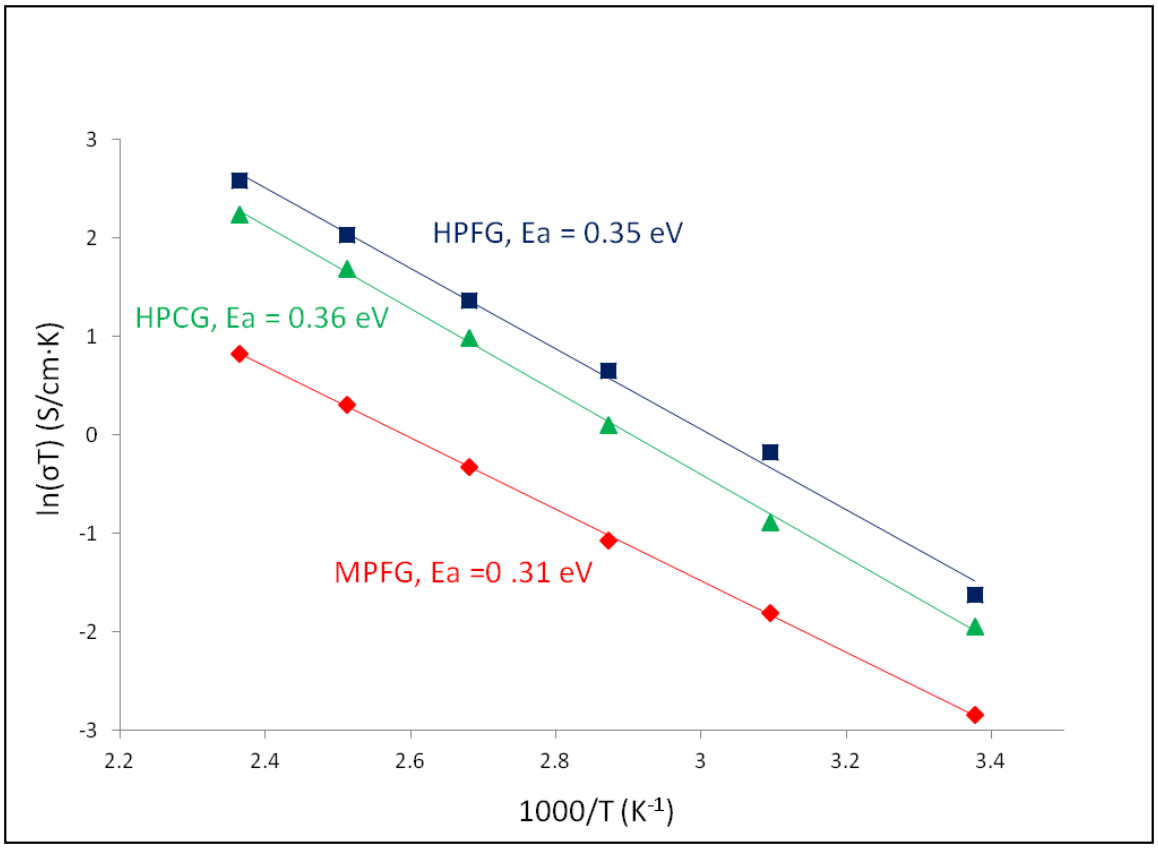

Figure 2.9. Arrhenius plot of ionic conductivity for MPFG, HPCG, and HPFG LATP.

Table 2.4

Ionic Conductivity of LATP from 298 – 423K

	σ_b (mS cm^{-1})			σ_{gb} (mS cm^{-1})			σ_t (mS cm^{-1})		
T (°C)	MPFG	HPCG	HPFG	MPFG	HPCG	HPFG	MPFG	HPCG	HPFG
25	6.88	6.39	9.56	0.20	0.53	0.72	0.20	0.49	0.67
50	39.33	24.46	36.28	0.52	1.35	2.80	0.51	1.28	2.60
75	46.16	37.84	62.85	1.01	3.51	6.05	0.99	3.20	5.52
100	44.79	47.51	55.95	2.03	8.45	12.90	1.94	7.17	10.48
125	42.69	40.68	41.74	3.73	20.46	35.85	3.43	13.61	19.28
150	43.67	38.93	36.10	6.20	51.63	241.92	5.43	22.19	31.41

microcracking. It has been shown that for dense ceramic materials, grain boundary impedance is inversely related to grain size [34,35]. This trend is overshadowed, however, when ion movement is hindered by microcracks that are very large on the atomic scale, providing boundaries of void space through which ions cannot travel.

An effort was made by Leach to use impedance spectroscopy as a way of determining the onset and effect of microcracking during the tetragonal to monoclinic transformation in YSZ, but he was not able to measure the effect [36]. Microcracks on this scale (only visible with TEM) may not play a large role in ionic conductivity, but the present results with LATP indicate that when the extent of the cracking is measurable using strength, dilatometry, and modulus measurements, there is a pronounced increase in grain boundary impedance.

With the bulk conductivity being generally the same for all specimens and impedance at the grain boundary dominating the total conductivity, an increase in conductivity correlating with a decrease in grain size is likely explained by the reduction of grain boundary microcracks. It follows, then, that a dense sample free of microcracks would have the optimal ionic conductivity, with any further reduction in grain size resulting in an increase in grain boundary impedance.

The activation energy for all three materials was in the range of 0.31-0.36 eV, being on the lower end of the 0.3-0.5 eV range [37,38]. The 0.67 mS cm^{-1} overall ambient temperature conductivity reported here is in excellent agreement with the 0.7 mS cm^{-1} conductivity originally reported by Aono et al. in 1989 [8], but is higher than many recent reports and is coupled with an activation energy higher than the 0.2 -0.3 eV range

Aono measured. Thus, conductivity at elevated temperatures was found to be higher than previously reported.

Ionic conductivity measured via a.c. impedance, however, does not take into account all of the impedances introduced in most practical electrochemical cells, which require d.c. measurements to confirm the a.c. measurements. HPFG membranes were used in an aqueous testing cell to measure d.c. conductivity. The cell operated at an average voltage of 3.5 V and was stable enough to have confidence in the d.c. conductivity value measured to be 1.61 mS cm^{-1}. This is lower than the 2.60 mS cm^{-1} total ionic conductivity at 50°C measured using the a.c. impedance method, but the 34% decrease is likely due to interfacial resistances in the system.

Several iterations of d.c. conductivity measurements showed that long-term testing of LATP materials in an aqueous LiOH environment was not possible due to rapid degradation of the membrane. The degradation appeared to be electrochemically driven, since under static conditions there did not appear to be any degradation. There is a need to determine the degradation mechanisms involved in aqueous environments for LATP.

2.5 Conclusions

While the single-most important factor in increasing the ionic conductivity in LATP-based solid electrolytes is clearly the elimination of high impedance secondary phases, which preferentially migrate to the grain boundaries, microcracking also lowers the conductivity of these materials when cracking is evident by Young's modulus measurements or using an SEM. Since the critical grain size for microcracking of $Li_{1.3}Al_{0.3}Ti_{1.7}(PO_4)_3$ is estimated to be less than or equal to 1.6 μm, very fine grains are required to avoid microcracked grain boundaries. None of the four experimental

materials tested in this study satisfied this requirement when considering the largest grains in the microstructure. The bulk conductivity was virtually constant between LATP that was phase-pure and LATP with secondary phases. The key to both improved strength and enhanced ionic conductivity in LATP materials will be processing a phase-pure ceramic with all grains below the critical size for microcracking.

While none of the materials tested in this study had all grains at or below the critical size, the benefits of microcrack reduction were shown with thermal expansion, strength, and ionic conductivity measurements. The biaxial and flexural strengths measured were 123±17 MPa and 147±14 MPa, respectively, for phase-pure, high-purity, fine-grained LATP. While these strengths are still low for ionically conducting ceramics like cubic zirconia, they were more than double the strength of LATP with secondary phases. The bulk fracture toughness of LATP was measured to be 1.1±0.3 MPa$\sqrt{m}$, which allowed the defect size to be determined. Defects were on the order of 30 μm for the best material and were not linked to microcracks, suggesting that further improvements in strength are possible.

The most important result of this work is the clear evidence that microcracking led to decreased conductivity due to increased impedance at grain boundaries. While no transmission electron microscopy was performed to determine if grain boundaries were devoid of secondary phases, comparison of similar purity materials clearly showed conductivity increasing with decreasing grain size. Increases in both conductivity and strength appear to be possible for LATP by a further reduction in grain size. High-purity, fine-grained LATP had the highest total ionic conductivity at all temperatures, measuring 0.67 mS cm^{-1} under ambient conditions with an activation energy of 0.35 eV.

Improvements in grain boundary conductivity are not presumed to be an improvement in the actual conductivity of the material found at grain boundaries in LATP, but a reduction in void spaces through which Li-ions cannot be conducted. Although the observation of lowered ionic conductivity due to microcracking is intuitive, it has never been shown that microcracking is a serious concern for the ionic conductivity of LATP ceramics. Microcracking should be avoided not only from a strength perspective, but from the standpoint of ionic conductivity.

2.6 References

1. M.S. Whittingham, "Electrical Energy Storage and Intercalation Chemistry," *Science* **192** (1976) 1126-1127.

2. B.C.H. Steele, "Fast Ion Transport in Solids: Solid-State Batteries and Devices," North-Holland/American Elsevier, Inc., Amsterdam-London/New York, (1973) 103.

3. L. Hagman and P. Kierkegaard, "The Crystal Structure of $NaMe_2^{IV}(PO_4)_3$; Me^{IV}=Ge, Ti, Zr," *Acta Chem. Scand.* **22** (1968) 1822-1832.

4. H.Y.P. Hong, "Crystal Structure and Crystal Chemistry in the System $Na_{1+x}Zr_2Si_xP_{3-x}O_{12}$," *Mater. Res. Bull.* **11** (1976) 173-182.

5. H.YP. Hong, J.A. Kafalas, and M. Bayard, "High Na^+-ion Conductivity in $Na_5YSi_4O_{12}$," *Mater. Res. Bull.* **13** (1978) 757-761.

6. J.B. Goodenough, H.Y.P. Hong, and J.A. Kafalas, "Fast Na^+-ion Transport in Skeleton Structures," *Mater. Res. Bull.* **11** (1976) 203-220.

7. J.B. Goodenough, "NASICON I Structure and Conductivity," *Solid State Ionics* **9/10** (1983) 793-794.

8. H. Aono, E. Sugimoto, Y. Sadaoka, N. Imanaka, and G. Adachi, "Ionic Conductivity of the Lithium Titanium Phosphate ($Li_{1+x}M_xTi_{2-x}(PO_4)_3$, M=Al, Sc, Y, and La) Systems," *J. Electrochem. Soc.* **136** (1989) 590-591.

9. J.W. Fergus, "Ceramic and Polymeric Solid Electrolytes for Lithium-ion Batteries," *J. Power Sources* **195** (2010) 4554-4569.

10. T. Oota and I. Yamai, "Thermal Expansion Behavior of NaZr2(PO4)3 Type Compounds," *J. Am. Ceram. Soc.* **69** (1986) 1-6.

11. J. J. Cleveland and R.C. Bradt, "Grain Size/Microcracking Relations for Pseudobrookite Oxides," *J. Am. Ceram. Soc.* **61** (1978) 478-481.

12. R.C. Bradt, "The Critical Grain Size for Microcracking in Low Thermal Expansion Anisotropic Ceramics," *Ceram. Trans.* **52** (1995) 5-18.

13. C.Y. Huang, D.K. Agrawal, and H.A. McKinstry, "Thermal Expansion Behavior of M'Ti2P3O12 (M'=Li, Na, K, Cs) and M"Ti4P6O24 (M"=Mg, Ca, Sr, Ba) Compounds," *J. Mater. Sci.* **30** (1995) 3509-3514.

14. D.A. Woodcock and P. Lightfoot, "Comparison of the Structure Behavior of the Low Thermal Expansion NZP Phases $MTi_2(PO_4)_3$ (M=Li, Na, K)," *J. Mater. Chem.* **9** (1999) 2907-2911.

15. H.L. Tuller, "Ionic Conduction in Nanocrystalline Materials," *Solid State Ionics* **131** (2000) 143-157.

16. J.P. Singh, A.V. Virkar, D.K. Shetty, and R.S. Gordon, "Strength-Grain Size Relations in Polycrystalline Ceramics," *J. Am. Ceram. Soc.* **62** (1979) 179-183.

17. M.S. Sygnatowicz, "Increasing the Strength of NaSICON Through Improved Processing," Senior Thesis, University of Utah (2007).

18. H. M. Rietveld, "A Profile Refinement Method for Nuclear and Magnetic Structures," *J. Appl. Crystallogr.* **2** (1988) 65-71.

19. ASTM C1499-09, "Standard Test Method for Monotonic Equibiaxial Flexure Strength of Advanced Ceramics at Ambient Temperature" (ASTM, Philadelphia, PA, 2009).

20. W. Weibull, "A Statistical Distribution Function of Wide Applicability," *J. Appl. Mech. Trans. ASME* **18** (1951) 293-297.

21. ASTM C1161-02c, "Standard Test Method for Flexural Strength of Advanced Ceramics at Ambient Temperature" (ASTM, Philadelphia, PA, 2008).

22. ASTM 1421-10, "Standard Method of Measuring Fracture Toughness of Advanced Ceramics at Ambient Temperature" (ASTM, Philadelphia, PA. 2010).

23. P.J. Gellings and H.J.M. Bouwmeester, *CRC Handb. Solid State Electrochem.* (1996).

24. J. Kuwano, N. Sato, M. Kato, and K. Takano, "Ionic Conductivity of $LiM_2(PO_4)_3$ (M=Ti, Zr, Hf) and Related Compositions," *Solid State Ionics* **70/71** (1994) 332-336.

25. A.S. Best, K.M. Nairn, P.J. Newman, D.R. MacFarlane, M. Forsyth, and M.J.G. Jak, "The Effect of Additives on Ceramic Materials for Lithium Solid Electrolytes," *J. Austral. Ceram. Soc.* **34** (1998) 236-241.

26. B. Kumar, S. Nellutla, J.S. Thokchom, and C. Chen, "Ionic Conduction Through Heterogeneous Solids: Delineation of the Blocking and Space Charge \Effects," *J. Power Sources* **160** (2006) 1329-1335.

27. P.W. Voorhees, "The Theory of Ostwald Ripening," *J. Stat. Phys.* **39** (1985) 231-252.

28. V. Tvergaard and J. W. Hutchinson, "Microcracking in Ceramics Induced by Thermal Expansion or Elastic Anisotropy," *J. Am. Ceram. Soc.* **71** (1988) 157-166.

29. S. Limaye and R. Nageswaran, NZP Final Report for LoTEC, Inc (1994).

30. G. Harshe, D. Agrawal, and S. Limaye, "High-Temperature Mechanical Properties and Chemical Stability of $Ba_{1+x}Zr_4P_{6-2x}Si_{2x}O_{24}$ Low-Thermal-Expansion Ceramics," *J. Am. Ceram. Soc.* **77** (1994) 1965-1968.

31. Yamai and T. Oota, "Grain Size-Microcracking Relation for NaZr2(PO4)3 Family Ceramics," *J. Am. Ceram. Soc.* **76** (1993) 487-491.

32. R. W. Rice and R.C. Pohanka, "Grain-Size Dependence of Spontaneous Cracking in Ceramics," *J. Am. Ceram. Soc.* **62** (1979) 559-563.

33. W.H. Rhodes, "Agglomerate and Particle Size Effects on Sintering Yttria-Stabilized Zirconia," *J. Am. Ceram. Soc.* **64** (1981) 19-22.

34. P. Mondal, A. Klein, W. Jaegermann, and H. Hahn, "Enhanced Specific Grain Boundary Conductivity in Nanocrystalline Y_2O_3-stabilized Zirconia," *Solid State Ionics* **118** (1999) 331-339.

35. M.K. Balapanov, E.K. Urazaeva, I.B. Zinnurov, R.S. Musalimov, and R.A. Yakshibaev, "Influence of Grain Sizes on the Ionic Conductivity and the Chemical Diffusion Coefficient in Copper Selenide," *Ionics* **12** (2006) 205-209.

36. C. Leach, "Microcrack Observations Using A.C. Impedance Spectroscopy," *J. Mater. Sci. Lett.* **11** (1992) 306-307.

37. P. Knauth, "Inorganic Solid Li-Ion Conductors: An Overview," *Solid State Ionics* **180** (2009) 911-916.

38. K. Arbi, J.M. Rojo, and J. Sanz, "Lithium Mobility in Titanium Based Nasicon $Li_{1+x}Ti_{2-x}Al_x(PO_4)_3$ and $LiTi_{2-x}Zr_x(PO_4)_3$ Materials Followed by NMR and Impedance Spectroscopy," *J. Eur. Ceram. Soc.* **27** (2007) 4215-4218.

3. STABILITY OF NASICON-TYPE $Li_{1.3}Al_{0.3}Ti_{1.7}P_3O_{12}$ IN AQUEOUS SOLUTIONS

3.1 Abstract

The chemical and electrochemical stability of high-purity lithium aluminum titanium phosphate (LATP) as a solid state electrolyte and physical separator in aqueous electrochemical cells was evaluated using LiOH, LiCl, $LiNO_3$, and $LiCOOCH_3$ salts as the Li source. LATP, with formula $Li_{1.3}Al_{0.3}Ti_{1.7}P_3O_{12}$, was found to be most stable between pH 8–9, with the longest cell operating continuously at 25 mA cm^{-2} for 625 hours at 40°C in $LiCOOCH_3$. Biaxial strength was 191 ± 11 MPa when tested in mineral oil, 144 ± 13 MPa as measured in air, and 26 ± 7 MPa after exposure to deionized water, suggesting that LATP undergoes stress-corrosion cracking. After exposure to LiOH, the strength was 76 ± 19 MPa. The decrease in strength was observed despite there being no measureable change in a.c. impedance spectra, X-ray diffraction, or sample mass, suggesting phosphate glasses at grain boundaries. At pH values outside of the 7–10 range, eventual membrane degradation was observed in all aqueous systems under electrochemical conditions. While LATP was surprisingly resistant to static corrosion in a hot, aqueous LiOH solution, electrochemical degradation was observed at the cathode due to subsurface pitting. Strength measurements were more instructive than impedance measurements in detecting this degradation.

3.2 Introduction

There is an ongoing research and development effort to develop a Li-ion battery that exhibits high energy capacity and cyclability while overcoming the limited temperature range and safety concerns inherent to organic electrolyte and polymer-based batteries that currently dominate the market [1-3]. This is of specific concern for large-scale batteries used in electric vehicles [4-7] and industrial-scale power storage [8,9]. Li et al. [10] introduced the first aqueous rechargeable Li-ion battery in 1994 which would have a clear advantage over their nonaqueous counterparts in terms of being safer, cheaper, and more environmentally friendly [11-15]. Since then, a significant effort has been focused on an aqueous alternative to the current battery configuration using water-stable Li-ion conductors as the positive and/or negative electrodes [13,16-23].

Due to the narrow electrochemical stability range of water, electrode materials for an aqueous Li-ion battery must be chosen carefully. Lithium titanium phosphate (LTP), with chemical formula $LiTi_2P_3O_{12}$, is a Li-ion conducting material from the sodium zirconium phosphate (NZP) family being considered as a negative electrode material in aqueous Li-ion batteries [16, 24-28]. It has an open-circuit potential of 2.5 V with respect to Li metal, which is below the 2.6 V decomposition potential of aqueous electrolytes at standard temperature and pressure [19] and has good electrochemical stability in water over a pH range of 7–9 [16,28]. However, LTP has significantly lower conductivity than the Al-doped lithium aluminum titanium phosphate (LATP) first reported by Aono et al. [29] with composition $Li_{1.3}Al_{0.3}Ti_{1.7}P_3O_{12}$. LATP possesses adequate ionic conductivity in an aqueous electrochemical cell to be used in many electrochemical applications, including as an electrode material in aqueous Li-ion batteries and as a Li transporting separator for aqueous stream purification and

concentration [30-32]. However, it has often been reported in the literature that LATP is not water stable, and although stability has been enhanced with slight additions of Si at the P site according to $Li_{1+x+y}Al_xTi_{2-x}Si_yP_{3-y}O_{12}$, where x is ~0.25 and y is 0.1 – 0.3 [33-35], these materials still exhibited poor stability in water and degraded in alkaline solutions, namely LiOH, after even short exposure times [36-38].

If long-term stability of LATP could be demonstrated under electrochemical conditions in aqueous media, especially in inexpensive solutions such as LiOH, it could lead to several applications, including aqueous Li-ion batteries. In many studies, LATP has been determined to be stable or instable in a given media due solely to changes in XRD patterns and/or a.c. impedance spectra. The objectives of the present study were to: 1) compare the d.c. conductivity of LATP in various Li salts, at the same Li^+ content, in aqueous solutions tested at 40°C; 2) use strength measurements on ceramic membranes as a means of monitoring electrochemical degradation; and 3) identify parameters which allow LATP to be used in aqueous environments.

3.3 Experimental

3.3.1 Characterization of Physical Properties

All testing was performed on high-purity LATP ($Li_{1.3}Al_{0.3}Ti_{1.7}P_3O_{12}$) specimens [30] that were obtained from Ceramatec, Inc. (Salt Lake City, Utah). Crystalline phases present were identified using an X-ray diffractometer (Philips model PW3040). Scans were conducted with Cu K_α radiation over a 2θ range of 15-75° using a step size of 0.02° and a 0.05 s dwell time. Density based on Archimedes' principle was measured in

isopropyl alcohol. The microstructure was examined using a scanning electron microscope (JEOL model JSM-5900LV SEM).

3.3.2 Static Corrosion Measurements

Sintered pellets with a 15 mm diameter and 5 mm thickness were used to measure the corrosion rate of LATP as a function of time in saturated aqueous LiOH at 65°C (3 pellets) and at the boiling point, or $T \sim 105$°C (5 pellets). Pellets at 65°C were placed in an HDPE bottle with 500 ml of solution and the change in mass of the pellets was recorded after 1, 4, and 7 week intervals. Pellets at 105°C were continuously boiled in 1000 ml of solution inside a glass bulb connected to a reflux unit with a water-chilled condenser tube. Pellet mass loss/gain measurements were taken at 1 and 4 week intervals. Corrosion rate was taken to be the mass loss/gain in mg per cm^2 per 100 hours.

3.3.3 Ionic Conductivity Measurements

3.3.3.1 A.c. conductivity. Pellets used in static corrosion testing in boiling LiOH were used for solid state a.c. impedance measurements before and after 4 weeks of exposure to boiling LiOH. Gold electrodes were sputtered onto both sides of the pellets with a sputter coater (Fullam EffaCoater) and a 'best fit circle' technique was used to analyze Nyquist plots to determine the bulk, grain boundary, and total ionic conductivity. A.c. impedance measurements were also taken on a 25 mm by 1 mm thick membrane used for d.c. testing in an aqueous $LiNO_3$ solution to investigate any change in a.c. impedance as a function of operating time. All measurements were made with a spectrometer (Solartron model SI 1260 Impedance/Gain-Phase) at an a.c. amplitude of 40 mV over a frequency range of 100 Hz to 10 MHz at room temperature.

3.3.3.2 D.c. conductivity. Electrochemical testing was conducted using the cell setup shown in Figure 3.1 to determine the performance and conductivity of the 25 mm diameter by 1 mm thick LATP membranes for 30 hours under d.c. conditions. The test cell had ethylene propylene diene monomer (EPDM) gaskets between the spacers and membrane scaffold and o-rings to seal and isolate the anode and cathode compartments. Using LiOH, LiCl, $LiNO_3$, and $LiCOOCH_3$ as Li salts for the aqueous electrolytes, solutions were maintained at approximately 2.0 wt% Li content regardless of the salt used. The Na concentration in each solution and the deionized water used to make the solutions was measured using inductively coupled plasma (ICP) analysis.

Tests were conducted at 40°C with a current density of 25 mA cm^{-2} using a Pt anode and Ni cathode, with a peristaltic pump being used to maintain a flow rate of ~500 ml/min through polypropylene tubing. Commercial software (*Labview*) was used to collect the voltage and current readings at 30 second intervals throughout the duration of each test. Tests were conducted with electrolytes in one of three possible configurations: 1) common flask – anolyte and catholyte drawn from and returned to a common source, 2) separate flask – anolyte and catholyte compartments kept separate from each other, or 3) separate flask, pH controlled – same as separate flask but with pH maintained between desired values. The voltage due to reactions at the electrodes was measured in situ, but with no membrane separating the cathode and anode compartments to obtain a 'blank' reading. This was used to isolate the resistance across the membrane, including interfacial resistances, for d.c. conductivity calculations.

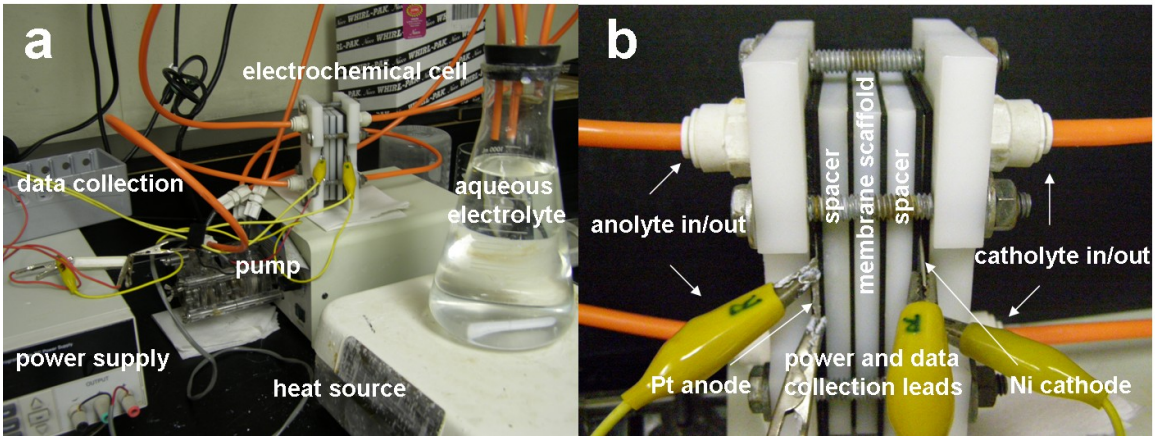

Figure 3.1. Pictures of (a) electrochemical testing setup used for d.c. conductivity and electrochemical corrosion measurements, and (b) the cell apparatus used for electrochemical tests.

3.3.4 Strength Measurements

The biaxial strength of specimens used in this study was determined using a universal testing machine (Instron model 5566) with a 1 kN load cell for the standard ring-on-ring test (ASTM C1499-04). The support structure had a radius on the compressive side of 6.5 mm and a radius on the tension side of 9.5 mm. A load was applied via a steel ball which was pressed against the top ring fixture through lowering a pushing rod attached to the testing machine at 0.5 mm/min with data collected every 50 ms. Tests were conducted in air, mineral oil, deionized water, and aqueous solutions of LiOH, LiCl, $LiNO_3$, and $LiCOOCH_3$. The pH of the deionized water was adjusted using NH_4OH to pH 9 to prevent ion exchange with hydronium ions. For measurements of specimens submerged in a solution, the bottom ring of the test fixture was taped to the bottom of a 50 ml Petri dish containing the liquid. Membranes for strength measurements were grouped into two categories: electrochemical and static. Electrochemical membranes were operated in a d.c. cell described above at 60°C for 16 hours in their respective solutions, while static membranes were suspended in the same

electrolyte solution in the d.c. cell without any potential being applied (except air, mineral oil, and deionized water specimens, which were held in air/solution at 60°C for 16 hours in a drying oven). The biaxial fracture strength was calculated as [39]

$$\sigma_f = \frac{3P}{2\pi t^2}\left[(1-\nu)\frac{D_S - D_L}{2D^2} + (1+\nu)ln\left(\frac{D_S}{D_L}\right)\right] \quad (3.1)$$

where P is the applied load, t is the specimen thickness, ν is Poisson's ratio, D_S and D_L are the support and load ring diameters, respectively, and D is the specimen diameter. Additional electrochemical strength measurements were made in LiOH at 60°C for 48 hours according to Equation (3.1) to investigate the difference in strength between the anode and cathode side of the electrochemically tested membranes.

3.4 Results

3.4.1 Physical Properties

Phase-purity of the as-received, high-purity LATP used for corrosion, strength, and electrochemical testing evaluated by XRD is depicted in Figure 3.2. All specimens were confirmed to be of the $Li_{1.3}Al_{0.3}Ti_{1.7}(PO_4)_3$ rhombohedral phase with no detectible secondary phases. The relative density of samples, calculated by dividing the bulk density by the theoretical density, was between 95–96%. Figure 3.3 is a representative SEM micrograph of the fracture and polished surfaces of a specimen, showing primarily intergranular fracture and a relatively fine microstructure [30].

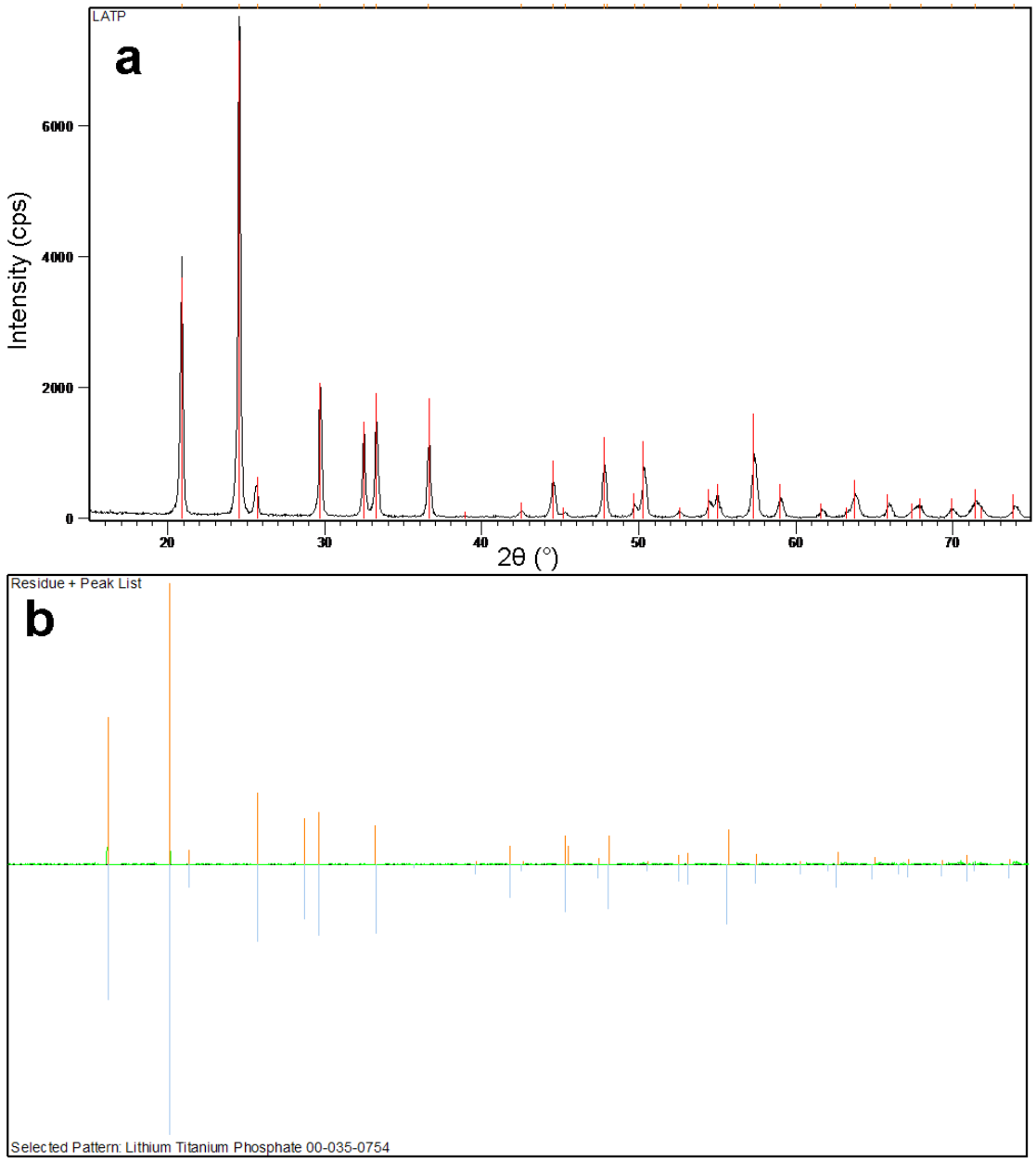

Figure 3.2. XRD patterns of high-purity LATP showing a) peak intensity and profile and b) a comparison with an indexed LTP pattern with rhombohedral NZP crystal structure.

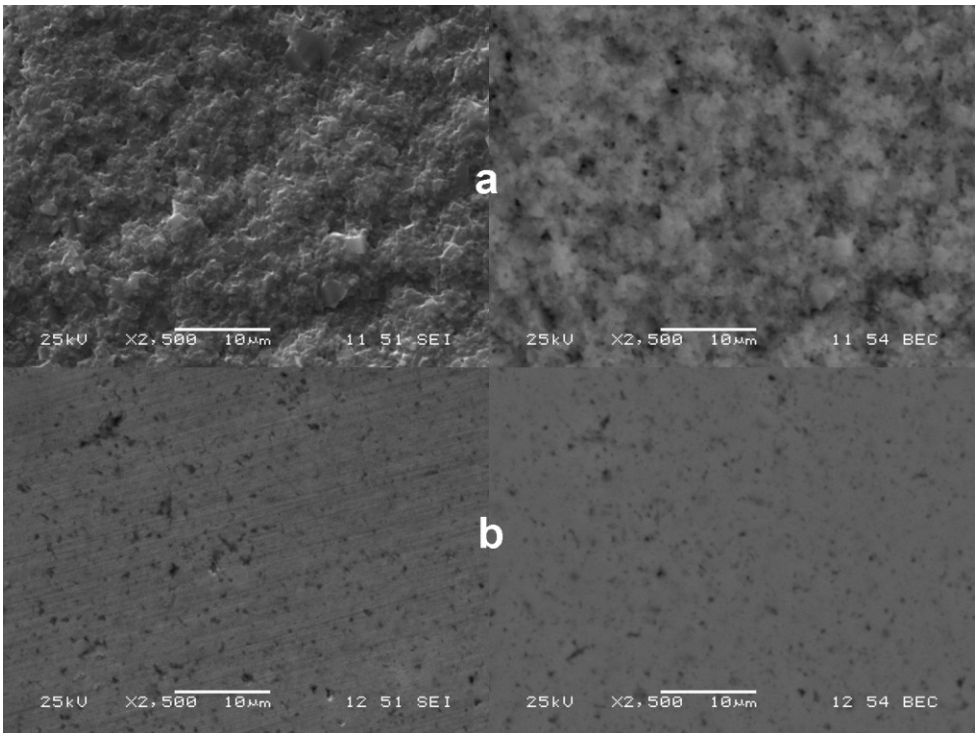

Figure 3.3. Secondary (left) and backscatter (right) SEM images of (a) a fracture surface and (b) a polished cross-section of high-purity LATP.

3.4.2 Static Corrosion Results

Table 3.1 provides the measured corrosion rate for the LATP pellets soaked in saturated aqueous LiOH for the specified time periods at 65°C or 105°C. It is evident that from a mass-change perspective, LATP would be considered extremely corrosion-resistant to LiOH. There is very little mass loss during the duration of the tests, and in one instance there is actually a slight gain in mass. This was confirmed to be the result of picking up Na (present as a low-level contaminant in LiOH powders) via ion exchange to form sodium titanium phosphate (NTP) at the surface, as seen in the XRD pattern in Figure 3.4. The micrographs also show no noticeable changes in the surface microstructure between a virgin pellet and the pellet soaked for 4 weeks in boiling LiOH. Also seen in the postcorrosion X-ray pattern is the fact that besides a slight shift from

Table 3.1

Measured corrosion rate of LATP in saturated LiOH solution

	Corrosion Rate (mg cm^{-2} 100 hr^{-1})		
	1 week	4 weeks	7 weeks
T = 65°C	0.04 ± 0.02	0.03 ± 0.01	0.02 ± 0.01
T ~ 105°C	-0.03 ± 0.03	0.01 ± 0.02	NA

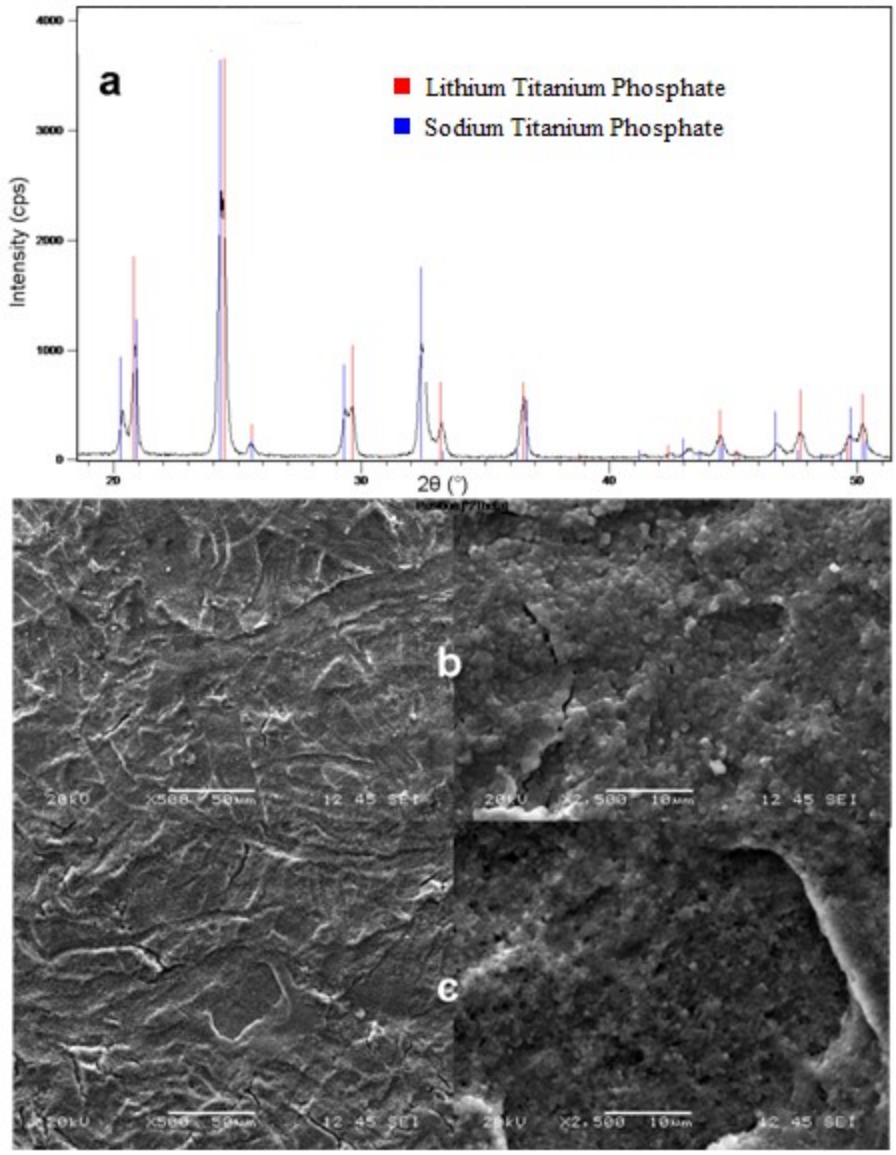

Figure 3.4. Results of LiOH static corrosion showing (a) an XRD pattern showing NTP formation in LATP as a result of Na^+ ion exchange, and SEM images of the surface of (b) a virgin LATP pellet and (c) an LATP pellet after 4 weeks of exposure to boiling saturated LiOH.

LATP to the sodium analogue, there does not appear to be any other secondary phases or decomposition of the LATP phase. Ion exchange is well known for NaSICON structures and Na^+ will exchange for Li^+ in LATP, causing cracking due to volume expansion. This behavior of Na-ion exchange into the LATP structure to form the sodium analogue always occurred in this study during tests involving aqueous solutions with some Na present, and is examined in more detail in subsequent sections.

3.4.3 Ionic Conductivity Results

3.4.3.1 A.c. conductivity. The Nyquist plot in Figure 3.5 provides the interesting result that there is no significant change in the a.c. impedance behavior between a virgin pellet and one boiled in saturated LiOH for 4 weeks. This, in conjunction with the lack of measurable mass-based corrosion, would indicate that LATP is stable in hot aqueous solutions of LiOH.

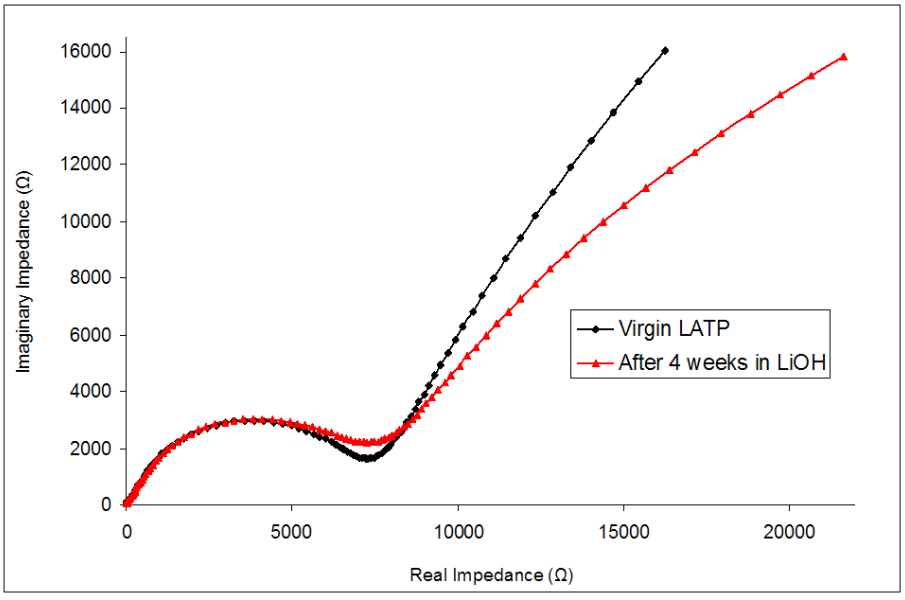

Figure 3.5. Nyquist plot used to calculate the solid state a.c. conductivity of LATP before and after 4 weeks of exposure to boiling, saturated LiOH.

A.c. impedance data of an LATP membrane tested under d.c. conditions (25 mA cm^{-2}) are shown in Figure 3.6. At first glance, it appears that there is a significant loss in conductivity as the test proceeds. However, this may be an artifact of the experimental procedure used. Materials in the NZP family show a tendency to hydrate and change their lattice parameters [40,41], and the membrane used for a.c. impedance measurements was thoroughly dried between each measurement, and thus the hydrated state was not tested.

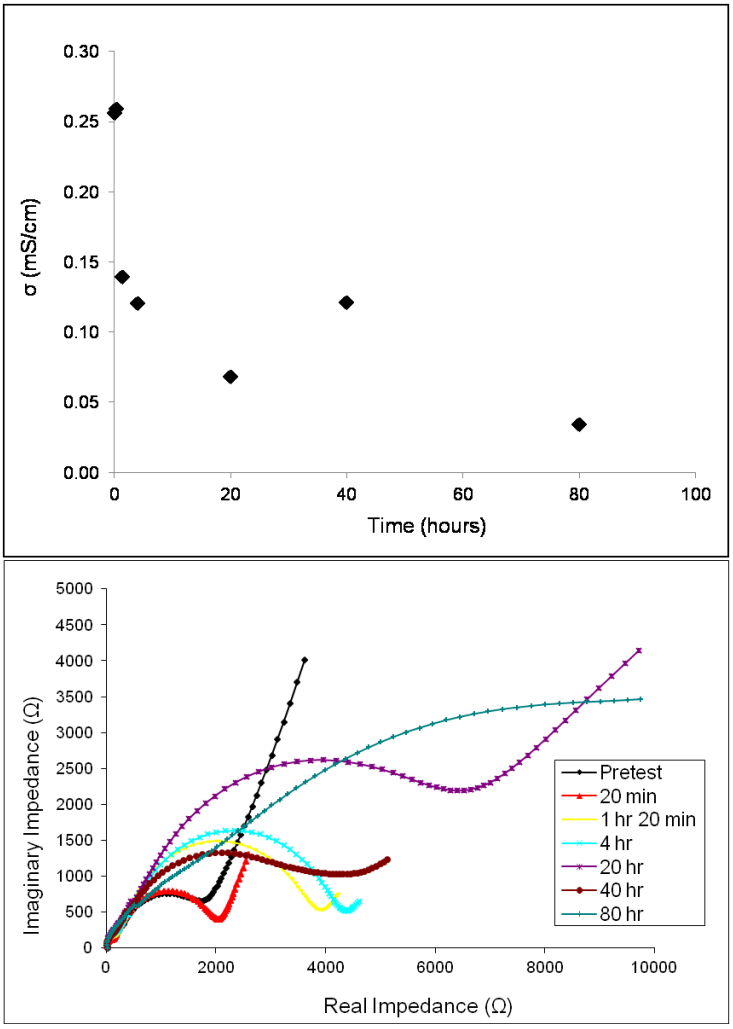

Figure 3.6. Results of an LATP in aqueous $LiNO_3$ d.c. electrochemical cell showing (a) the change in a.c. conductivity as a result of an applied current of 25 mA cm^{-2} at 40°C over time, and (b) Nyquist plots showing a change in the grain boundary conductivity.

In Figure 3.7, it is interesting to note that every time the membrane was dried, measured, and restarted there is an apparent 'break in' period of high voltage which eventually lowers and flattens out. This is most likely a rehydration period, which results in the ionic conductivity matching what was recorded in the voltage and current during the flat regions. Impedance measurements, as conducted using this approach, were a poor predictor of d.c. performance.

3.4.3.2 D.c. conductivity. D.c. conductivity results in the aqueous Li salt solutions are summarized in Table 3.2. Each cell operated at a different voltage due to differing half-cell reactions at the anode and cathode, but when these and other contributions to the total resistance were

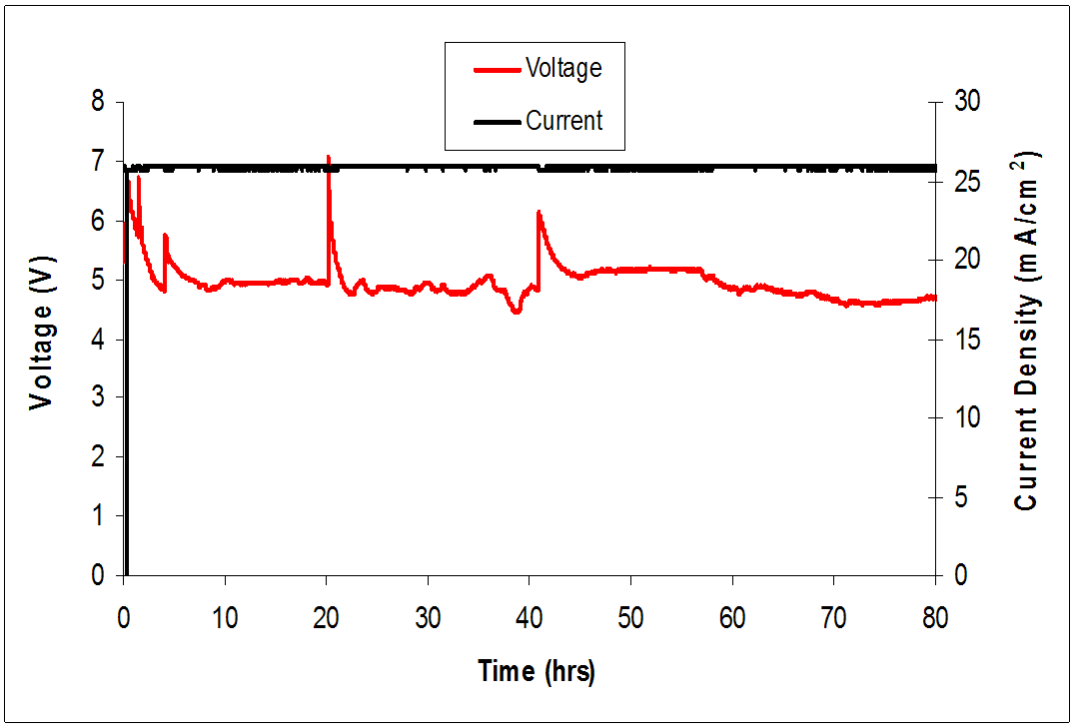

Figure 3.7. Voltage\current density versus time trace for an LATP membrane in aqueous $LiNO_3$ d.c. electrochemical cell used to measure the a.c. conductivity as a function of operation time at 25 mA cm^{-2} and 40°C.

Table 3.2

Membrane conductivity measured in d.c. electrochemical cells tested in a common flask configuration.

	LiOH	$LiNO_3$	$LiCOOCH_3$	LiCl
σ (mS cm^{-1})	1.7	1.8	1.1	1.5

taken into account, the calculated d.c. conductivity is in the range of 1.1 to 1.8 mS cm^{-1} for the different solutions tested. These values are much lower than the 2.4 mS cm^{-1} predicted by solid state a.c. impedance, in agreement with a previous test in LiOH [30]. Solid/liquid interfacial resistance to ion transfer lowers the conductivity and will undoubtedly be different between the solutions.

Figure 3.8 provides a graph of the current density and voltage as a function of time for a representative run of each aqueous Li salt solution tested in a common flask

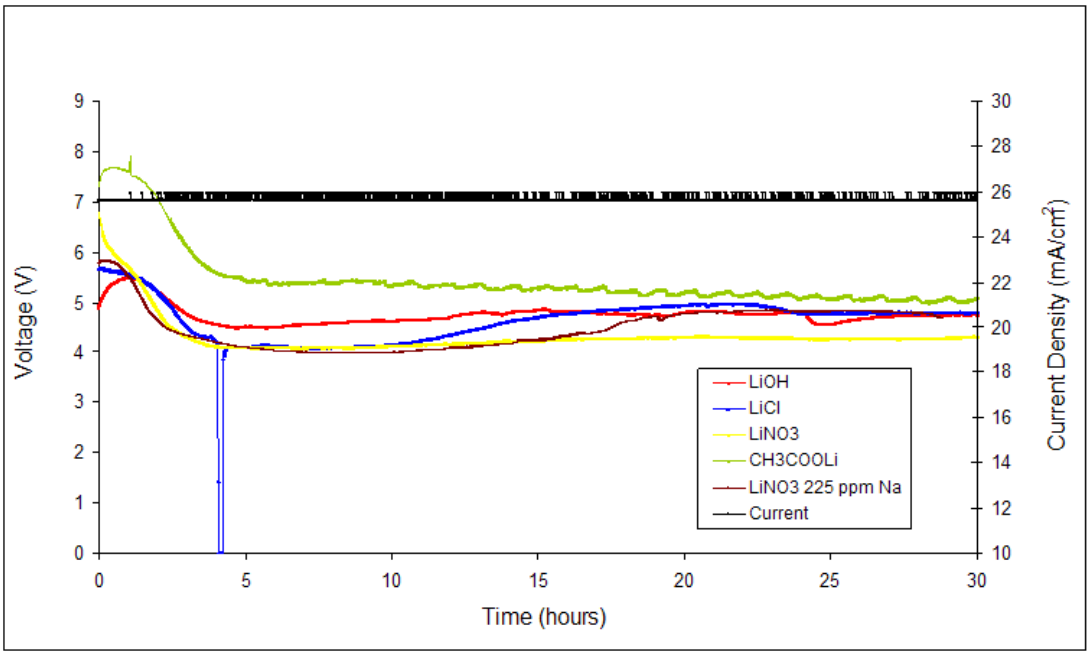

Figure 3.8. Voltage\current density versus time traces for LATP membranes in various aqueous Li salts with 25 mA cm^{-2} current density at 40°C.

scenario. Each cell was run for 30 hours, after which the membrane was analyzed for any signs of degradation. Again, a clear 'break in' period of ~4 hours is seen regardless of the solution.

The factor that had the most dramatic effect on the integrity of the membrane was found to be the concentration of Na contamination. The membrane run in LiCl solution was cracked and flaking upon cell disassembly, as seen in Figure 3.9. ICP analysis results, summarized in Table 3.3, showed that the LiCl solution contained ~220 ppm Na, which was much higher than the other three solutions. The degradation was confirmed as ion exchange by XRD analysis of failed membranes, showing significant formation of NTP (greater than that shown in Figure 3.4) which has a larger unit cell volume and will cause lattice expansion and cracking if the material is confined, such as the cell apparatus used. To confirm this effect, a known amount of $NaNO_3$ was added into a $LiNO_3$ solution (identical to that previously used) to bring the Na^+ level up to ~250 ppm

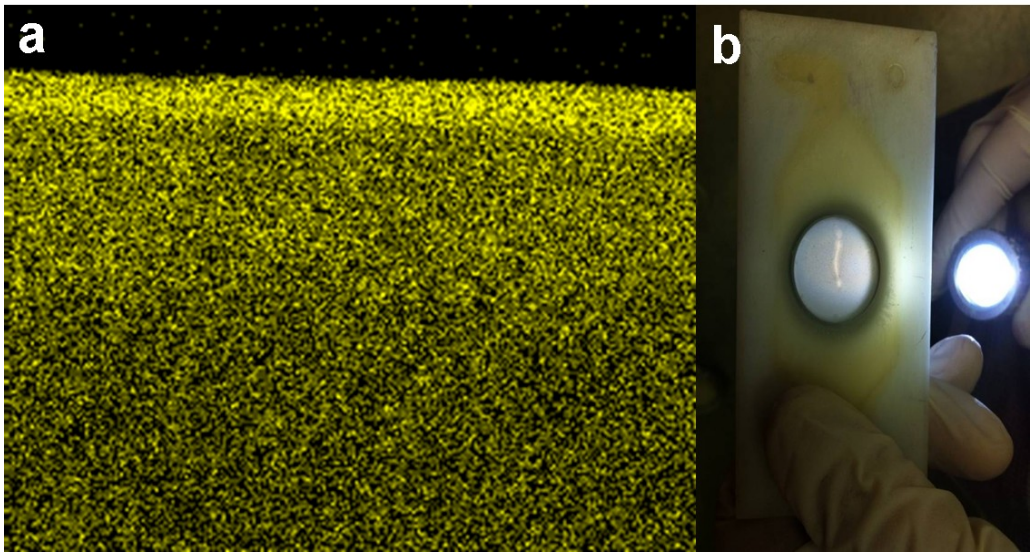

Figure 3.9. Results from a d.c. electrochemical cell using an LATP membrane in aqueous LiCl at 25 mA cm^{-2} and 40°C showing (a) cross-sectional EDS mapping of Na, and (b) a membrane cracked after short-term testing.

Table 3.3

Na concentration in aqueous Li salt solutions measured by ICP

	Deionized Water	LiOH	$LiNO_3$	$LiCOOCH_3$	LiCl	$LiNO_3$ + $NaNO_3$
Na (ppm)	<1	11	5	13	223	256
pH at 40°C	9.0	11.9	10.8	8.4	10.3	10.7

and the same test was repeated. The membrane in this test failed in a similar manner to the original LiCl membrane and XRD again confirmed the formation of NTP. Figure 3.9 also shows EDS analysis of the polished cross-section of the membrane run in $LiNO_3$ solution with ~250 ppm Na, showing a clear Na-rich surface layer and slight gradient into the material. Indeed, LATP proved extremely sensitive to ion exchange with Na, with detectable NTP formation after only 30 hours of operation occurring even in the solutions with ~10 ppm Na.

Membranes tested in LiOH showed degradation in the form of pitting and flaking on the cathode side of the membrane only, as shown in Figure 3.10. Subsequent runs confirmed this interesting result. In an effort to increase membrane longevity, a completely symmetric separate flask LiOH cell was run with Ni anode/cathode and the direction of current flow was manually switched every 24 hours, causing the anode and cathode sides of the membrane to alternate. The voltage and current traces for this run are given in Figure 3.11, showing the cell was able to operate for 215 hours, at which point the degradation on both sides of the membrane resulted in failure.

The $LiNO_3$ and $LiCOOCH_3$ systems did not fail and did not undergo any observable changes in physical appearance during the 30 hour tests. Longer-term runs in these two chemistries were performed, the longest of which was 625 hours of continuous

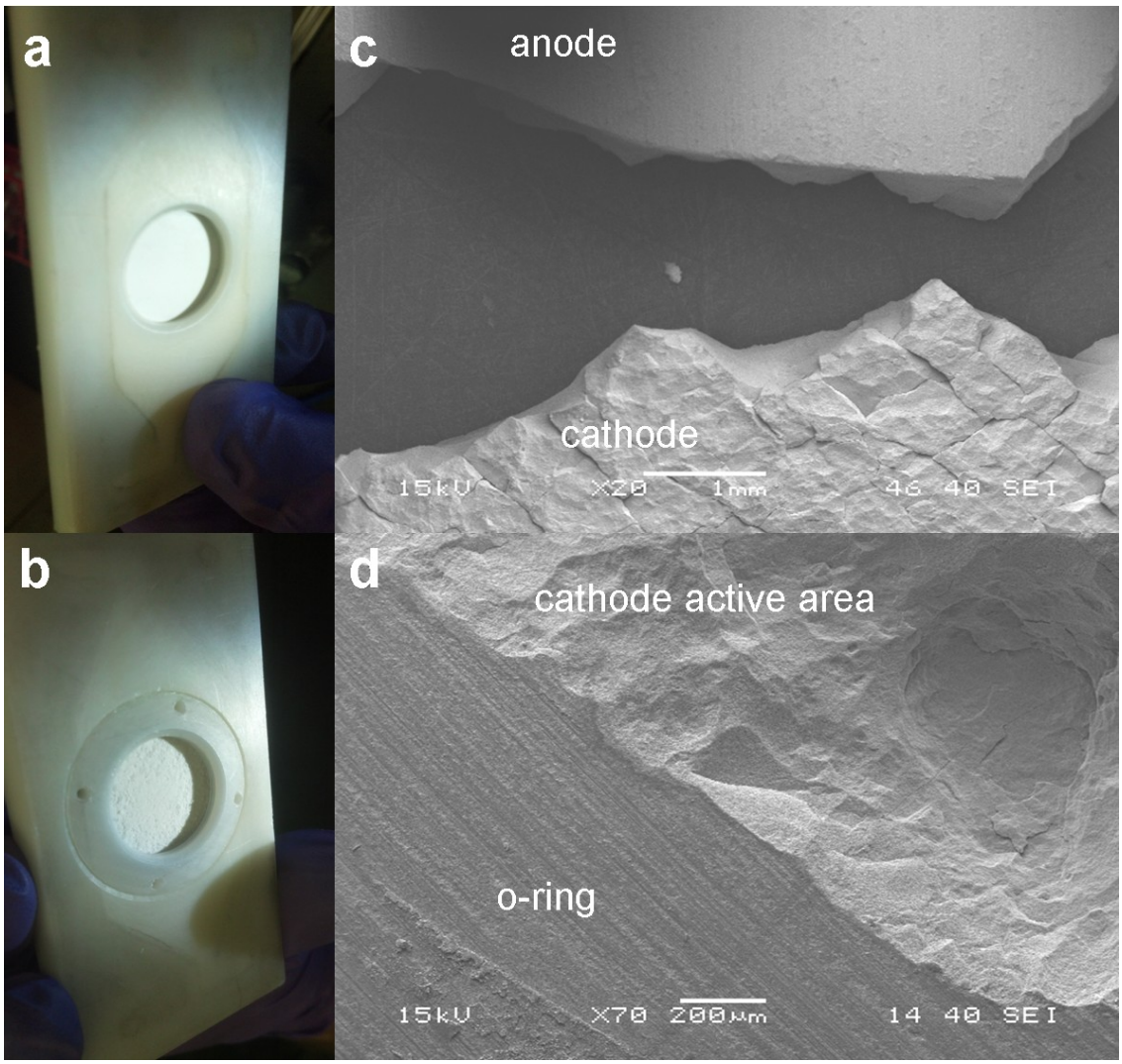

Figure 3.10. Results from a d.c. electrochemical cell using an LATP membrane in aqueous LiOH at 25 mA cm^{-2} and 40°C showing optical images of (a) anode and (b) cathode surfaces of the membrane after testing, and (c) an SEM comparison of anode and cathode surfaces with (d) a higher magnification image of pitting observed on the cathode side of the membrane.

operation without membrane failure in an aqueous $LiCOOCH_3$ solution and common flask configuration. The electrode reactions were such that a mole of acid and a mole of base were generated at the same rate, and therefore the solution was self-buffered at pH ~8. Upon disassembly, the membrane was a slightly off-white color on the anode side, but there was no visible pitting or cracking and posttest analysis revealed only Na-ion exchange consistent with other runs. Two other runs of >300 hours of cell operation

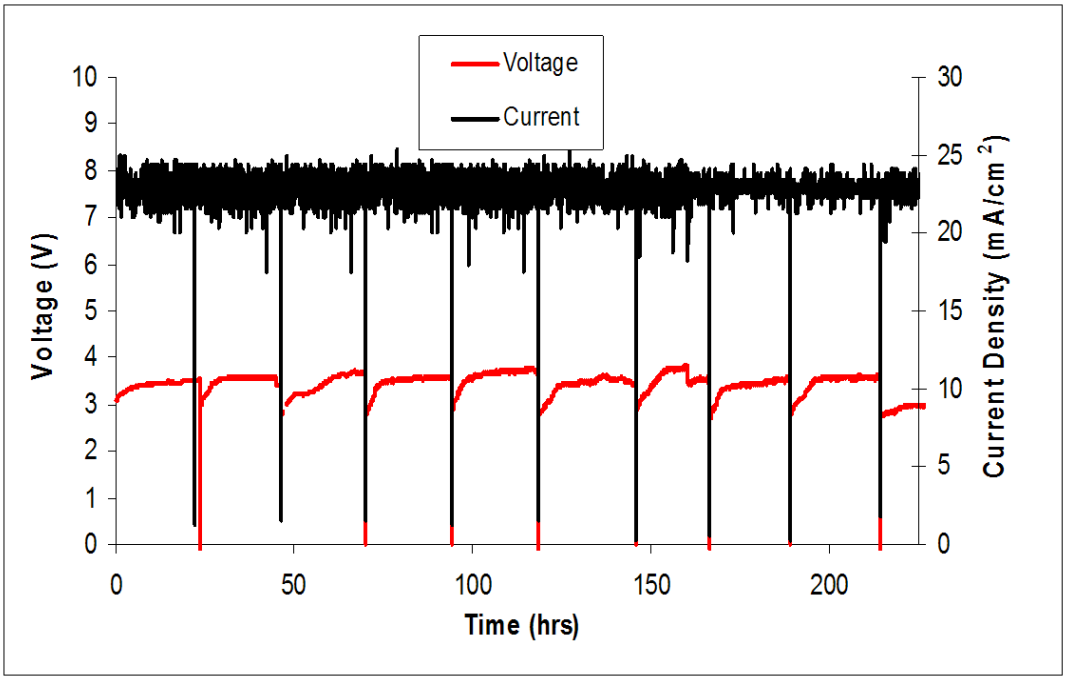

Figure 3.11. Voltage\current density versus time trace for an LATP membrane in aqueous LiOH d.c. electrochemical cell at 25 mA cm^{-2} and 40°C with the anode and cathode leads being reversed every 24 hours.

were performed in aqueous $LiNO_3$ in a common flask without membrane failure, but with slight formation of Li_3PO_4 on the anode side of the membrane. This formation was also detected during even short-term tests in LiCl solution, and in all cases appeared to form subsurface 'blisters', of which a severe case is shown in Figure 3.12.

It appears that if the Na concentration in the aqueous electrolyte is kept low, cell longevity is strongly dependent on the pH of the aqueous solutions. The terminal pH of each solution under a common flask configuration is given along with the Na content in Table 3.3. Low pH leads to H^+ ion exchange in LATP (and other materials from the NZP family) and is well-documented [36,42,43]. Instability in high pH, on the other hand, has not been as thoroughly addressed or understood. Using the separate flask and pH controlled separate flask configurations with $LiCOOCH_3$ solution, the effect of pH on cell longevity was investigated.

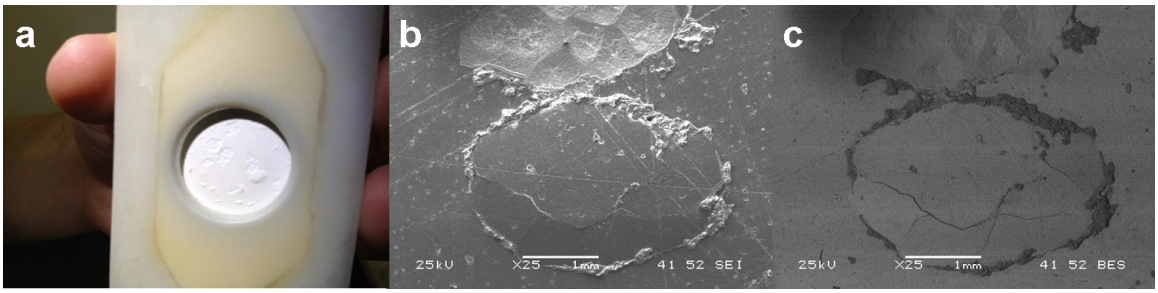

Figure 3.12. Subsurface Li_3PO_4 'blisters' on the anode side of an LATP membrane seen in an (a) optical image, (b) secondary SEM image, and (c) backscatter SEM image.

Figure 3.13 shows that when the compartments are kept separate and the anolyte and catholyte quickly become acidic and basic, respectively, the voltage rises quickly and the membrane fails. However, when the pH is maintained in the broad window of 6.5 – 11.5, cell longevity is greatly increased. This can then be compared with the self-buffered common flask run which lasted 625 hours with no failure (only initial 325 hours graphed for ease of comparison). The spikes in voltage at 75 and 110 hours proved to be Li_2CO_3 scaling on the cathode electrode, which once removed resulted in low voltage.

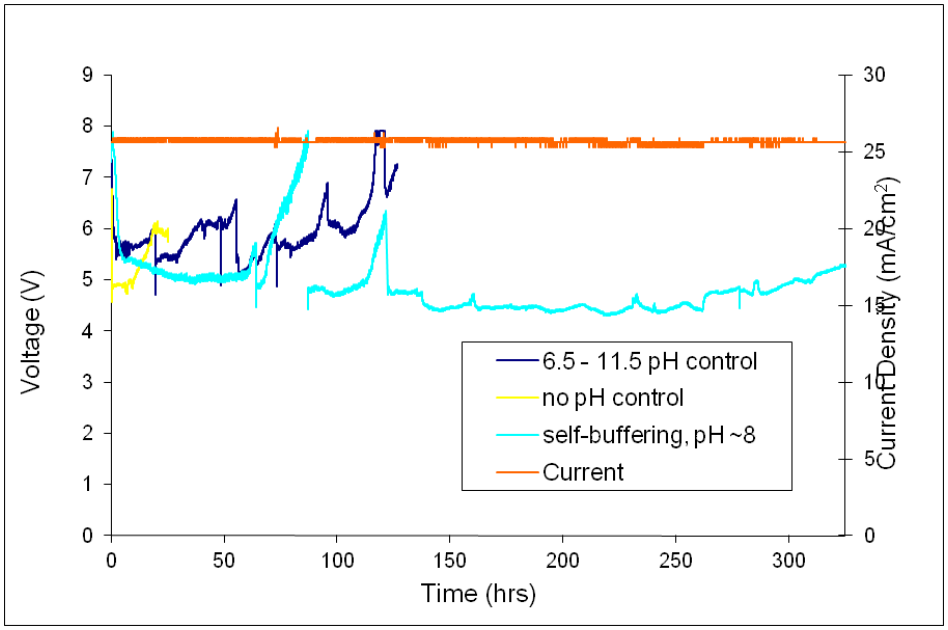

Figure 3.13. Voltage\current density versus time traces for LATP membranes run in aqueous $LiCOOCH_3$ solutions of differing pH at 25 mA cm^{-2} and 40°C.

3.4.4 Strength Results

Strength results are summarized in Tables 3.4 (static tests) and 3.5 (electrochemical tests). While the data are sparse, the results are quite surprising. The average biaxial strength measured for LATP was 144 MPa in air and 191 MPa in mineral oil. However, there is an 82% drop in strength to 26 MPa for LATP exposed to deionized water, despite no changes in the XRD patterns, mass, or impedance spectra. A comparison of static versus electrochemical tests showed little difference in $LiNO_3$ (35 versus 44 MPa) or $LiCOOCH_3$ (54 versus 46 MPa), with a strength decrease in LiOH (76 versus 49 MPa). The strength of LATP when exposed to aqueous solutions of Li salts varies, but is consistently much lower than the strength measured in air. Exposure to deionized water resulted in a much larger decrease in strength then the effects of operating in an electrochemical cell or being soaked in aqueous solutions of Li salts.

When LATP was removed from the holder and dried to allow X-ray diffraction measurements, the samples were noticeably stronger. Measurements showed that the strength of the dried membranes increased from 26 MPa to 59 MPa, consistent with a dehydration reaction. It is important to note that membranes soaked and run electrochemically in LiCl solution cracked prior to strength measurements.

Table 3.4

Biaxial strength (MPa) for LATP tested statically

	Air	Deionized Water, dried	Deionized Water	Mineral Oil	LiOH	LiCl	$LiNO_3$	$LiCOOCH_3$
LATP	144 ± 13 (5)	59 ± 19 (4)	26 ± 7 (13)	191 ± 11 (4)	76 ± 19 (7)	0 (4)	35 ± 8 (4)	54 ± 12 (4)

Number of samples tested is given in parentheses

Table 3.5

Biaxial strength (MPa) for LATP after electrochemical testing

	LiOH	LiOH (48 hours)		LiCl	$LiNO_3$	$LiCOOCH_3$
LATP	49 ± 10 (3)	41 ± 14 (A, 4)	17 ± 3 (C, 4)	0 (3)	44 ± 15 (3)	46 ± 4 (3)

Number of samples tested is given in parentheses. A=anode side in tension, C=cathode side in tension.

3.5 Discussion

The high-purity, fine-grained LATP had excellent strength (191 MPa) despite being microcracked [30] when tested in mineral oil so as to exclude moisture from the crack tip. Using the measured fracture toughness of 1.1 MPa√m [30], the calculated flaw size is only 20 μm, suggesting good processing for this LATP. When exposed to air, the flaw size increased to 35 μm under the same test conditions. Exposure to water resulted in at least an order of magnitude increase in flaw size. Even exposure to relatively dry air (relative humidity <60%) noticeably reduced the strength. Because XRD, a.c. impedance, mass change, and scanning electron microscopy were unable to detect any change, it is speculated that a grain boundary glass containing P is being subjected to slow-crack growth under stress. Phosphate glasses are prone to stress corrosion cracking [44,45], and strength is lowered at the crack tip in the presence of water, where the stress-enhanced chemical reactions are given as [46]

$$H_2O + P - O - P \rightarrow 2(P - OH) \quad (3.2)$$

$$H_2O + P - O - M \rightarrow P - OH + M - OH \quad (3.3)$$

where *M* is a metal cation. Equations (3.2) and (3.3) show how water can react with the *P – O – P* or *P – O – M* bonds, resulting in crack propagation. In this way, a significant reduction in strength could occur while being nearly undetectable via mass change measurements or XRD analysis.

The trend of membrane strength in static solutions was LiCl<<H2O<LiNO3< CH3COOLi<LiOH, as shown in Table 3.4. Ion exchange of Na+ for Li+ caused cracking of the LATP in LiCl. Neither the pH of the solution nor the Na+ content in the solutions correlate with the general trend in strength. One interesting observation is that the mechanical strength of LATP is highly correlated with the ratio of the concentration of salt divided by the maximum amount soluble at 40°C. This ratio is 0.66, 0.36, and 0.12 for LiOH, LiCOOCH3, and LiNO3, respectively. The higher the ratio, the stronger the attraction of the water is to the ions in solution. If one assumes that deionized water has a ratio of 0, a plot of LATP strength as a function of this ionic strength ratio is surprisingly linear (r^2=0.9997), as shown in Figure 3.14. These data suggest that a water-soluble lithium phase may be associated with the strength reduction. It was anticipated that strength could be used to see electrochemical degradation. A comparison of Tables 3.4 and 3.5 show that there was no difference in strength between LATP exposed to the electrochemical driving force and those in the same solution, but without current passing through them for both $LiNO_3$ and $LiCOOCH_3$ solutions. This may be the result of the short duration of the tests, but the ability of LATP to be tested for hundreds of hours in $LiCOOCH_3$ supports these data. Also, since there is evidence of hydration/dehydration reactions, it is important that the LATP sample not be constrained in the test set-up when

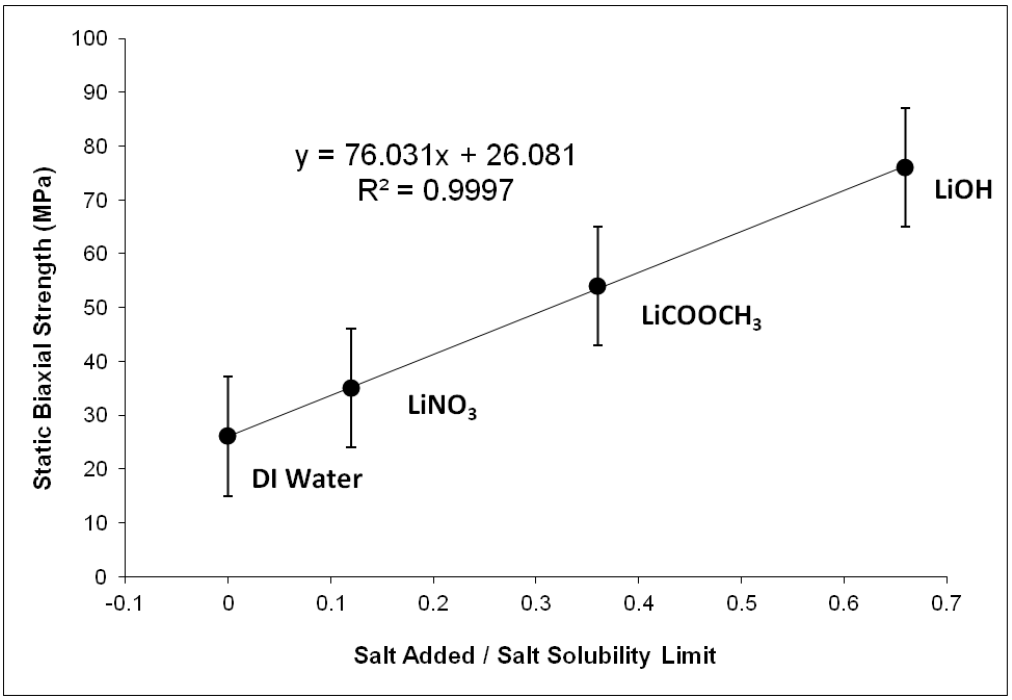

Figure 3.14. Biaxial strength of membranes tested statically as a function of the amount of salt solvated in water divided by the maximum soluble for various Li salts.

being dehydrated or rehydrated in order to avoid cracking of the membrane due to the accompanying volume change.

The electrode reactions for all tests were predominantly water splitting reactions at the Pt anode and Ni cathode. For LiOH solutions, they proceeded as

Anode: $$4OH^- \rightarrow O_2 + 2H_2O + 4e^-$$ (3.4)

Cathode: $$2H_2O + 2e^- \rightarrow H_2 + 2OH^-$$ (3.5)

while for the LiCl, $LiNO_3$, and $LiCOOCH_3$ solutions, they were given by

Anode: $$2H_2O \rightarrow O_2 + 4H^+ + 4e^-$$ (3.6)

Cathode: $$2H^+ + 2e^- \rightarrow H_2$$ (3.7)

For either case, the net reaction is

$$2H_2O \rightarrow 2H_2 + O_2 \quad (3.8)$$

Equation (3.9) gives a competing reaction at the Pt anode for the LiCl system as

Anode: $$2Cl^- \rightarrow Cl_2 + 2e^- \quad (3.9)$$

The cathodic reaction is the same as Equation (5), giving an overall reaction of

$$2Cl^- + 2H_2O \rightarrow H_2 + Cl_2 + 2OH^- \quad (3.10)$$

While Equation (3.9) is a secondary anode reaction for the LiCl solution, it does explain why the solution pH gradually rises as the test proceeds due to the lack of sufficient acid being produced to balance the hydroxide. This rise in pH continues until the production of hydroxide at the cathode and its subsequent oxidation at the anode according to Equation (3.4) are in equilibrium. The electrode reactions in a common flask scenario for the $LiNO_3$ and $LiCOOCH_3$ solutions are of sufficient complexity as to not be discussed in detail here, but it can be said that a competing gas formation reaction at the Pt anode in the $LiNO_3$ solution allowed for an overall rise in pH until it became buffered in the same manner as LiCl, while the electrode reactions in $LiCOOCH_3$ solution maintained a buffered pH of ~8.

For the membranes exposed to LiOH under electrochemical conditions, noticeable strength degradation occurred. Additional strength measurements were made to test the difference in strength between the cathode and anode side of the membrane in support of observed degradation (pitting) on the cathode side. Results supported the visual observations, with the strength when the cathode side was in tension being 61% lower on average than when the anode side was in tension. The reaction at the LiOH cathode produces hydroxyl ions, which are carried towards the cathode. One might expect attack at the surface of the LATP as opposed to the pitting which occurred, with fracture initiating within the sample as shown in Figure 3.10.

Interestingly, high pH appears to have little effect statically, but under a potential, it has a significant effect on the cathode (reducing) side of the membrane. This type of cathodic corrosion could be explained by a model recently proposed by Virkar [47-49], explaining that if the ionic and electronic currents through the membrane are in the same direction (which is the case for all electrochemical cells operated in this study), there is the possibility that the chemical potential of Li metal at the very surface of the membrane may be lower than that of a Li^+ ion during transport, causing local precipitation of Li at the membrane/electrolyte solution interface. This would lead to degradation consistent with the pitting observed on the cathode side of the membrane in LiOH cells. Recently, this model has been supported experimentally in solid oxide electrolyzer cells [50].

This instability at high pH was also confirmed for the $LiNO_3$ system by running a separate flask cell with a LiOH anolyte and $LiNO_3$ catholyte, thus preventing acidic conditions at the anode while allowing the cathode to experience increasingly basic conditions. As the cell operated, LiOH was produced at the cathode and the catholyte pH

changed from 7.6 to 11.3 over 72 hours, resulting in advanced pitting only on the cathode side of the membrane identical to that seen in a LiOH cell.

However, the fact that Li^+ could be transported for hundreds of hours without any evidence of pitting for cells run in a pH range of 8-9 does not support this model, nor did SEM observations, which failed to find Li metal precipitated at any of the freshly fracture pits on the cathode side of the membrane. This may indicate that the solution pH has an effect on transport parameters and the chemical potential of Li-ions versus Li metal.

Previous studies have suggested that NaSICON-type materials are unstable in water [40,41,43]. While NaSICON has been shown to have good stability in NaOH for long periods of time, this is the first study to suggest that LATP could be used in aqueous solutions if the pH could be controlled in a moderately basic pH range. While strength measurements show that water degrades the mechanical properties of this material to values lower than NaSICON, there is no indication that the degradation is catastrophic as long as ion exchange, which puts the anode side in compression and the cathode side of the membrane in tension, can be limited and the pH of the solution can be kept in the range of 7-10. Unfortunately, none of the salts tested satisfy this condition under desired operating conditions. For this reason, it is suggested that nonprotonic organic solvents be tested when using LATP as a membrane material.

3.6 Conclusions

When tested at the same Li^+ concentration (2 wt%) and current density (25 mA cm^{-2}) at 40°C in deionized water, $LiNO_3$ and LiOH solutions resulted in the highest conductivity in LATP membranes (~1.8 mS cm^{-1}) while LiCl was slightly lower (~1.5 mS cm^{-1}) and $LiCOOCH_3$ had the lowest conductivity (~1.1 mS cm^{-1}). Electrode

reactions resulted in high pH at the cathode and low pH at the anode, both of which are problematic for LATP. However, by using a common flask, which allowed for self-buffering in the case of $LiCOOCH_3$, it was possible to show that the LATP was stable over hundreds of hours of operation in the pH range of 8–9.

High-purity, fine-grained LATP [30] is susceptible to stress-corrosion cracking, with strength decreasing dramatically (191 MPa to 26 MPa) when exposed to water. The strength in salt solutions was highly correlated with the ability of water to solvate the salt, with LiOH showing the highest strength (76 MPa) in static solutions. In the case of LiOH, static testing showed that LATP could last for hundreds of hours in the same high pH (>11.5) that resulted in short-term cathodic pitting in electrochemical testing. It was also shown that changes in strength can be a more sensitive indicator of degradation than XRD and a.c. impedance measurements, evidenced here by the results of LATP in aqueous LiOH solutions.

In order for LATP to be used in aqueous solutions in electrochemical cells, two conditions must be satisfied for low-temperature (40-60°C) operation: 1) the pH must be maintained in the range of 7–10, and 2) the Na^+ concentration must be kept low to avoid ion exchange. There are no practical applications for LATP in aqueous solutions, but strength testing in mineral oil suggests that it may be worthwhile to look at this material in nonprotonic organic solvents used for electrochemical cells.

3.7 References

1. J.W. Fergus, “Ceramic and Polymeric Solid Electrolytes for Lithium-ion Batteries,” *J. Power Sources* **195** (2010) 4554-4569.

2. P. Knauth, “Inorganic Solid Li-Ion Conductors: An Overview,” *Solid State Ionics* **180** (2009) 911-916.

3. N. Anantharamulu, K.K. Rao, G. Rambabu, B.V. Kumar, V. Radha, and M. Vithal, "A Wide-ranging Review on Nasicon Type Materials," *J. Mater. Sci.* **46** (2011) 2821-2837.

4. A.D. Pasquier, I. Plitz, S. Menocal, and G. Amatucci, "A Comparative Study of Li-Ion Battery, Supercapacitor, and Nonaqueous Asymmetric Hybrid Devices for Automotive Applications," *J. Power Sources* **115** (2003) 171-178.

5. K.T. Chau, Y.S. Wong, and C.C. Chan, "An Overview of Energy Sources for Electric Vehicles," *Energy Conver. Manage.* **40** (1999) 1021-1039.

6. P.C. Frost, "Developments in Lead-acid Batteries: A Lead Producer's Perspective," *J. Power Sources* **78** (1999) 256-266.

7. P. Gifford, J. Adams, D. Corrigan, and S. Venkatesan, "Development of Advanced Nickel/Metal Hydride Batteries for Electric and Hybrid Vehicles," *J. Power Sources* **80** (1999) 157-163.

8. D.H. Doughty, P.C. Butler, A.A. Akhil, N.H. Clark, and J.D. Boyes, "Batteries for Large-scale Stationary Electrical Energy Storage," *J. Electrochem. Soc. Interface* (2010) 49-53.

9. T. Tanaka, K. Ohta, and N. Arai, "Year 2000 R&D Status of Large-scale Lithium Ion Secondary Batteries in the National Project of Japan," *J. Power Sources* **97-98** (2001) 2-6.

10. W. Li, J.R. Dahn, and D.S. Wainwright, "Rechargeable Lithium Batteries with Aqueous Electrolytes," *Science* **264** (1994) 1115-1118.

11. W. Li and J.R. Dahn, "Lithium-Ion Cells with Aqueous Electrolytes," *J. Electrochem. Soc.* **142** (1995) 1742-1746.

12. H.Q. Yang, D.P. Li, S. Han, N. Li, and B.X. Lin, "Vanadium-manganese Complex Oxides as Cathode Materials for Aqueous Solution Secondary Batteries," *J. Power Sources* **58** (1996) 221-224.

13. J. Kohler, H. Makihara, H. Uegaito, H. Inoue, and M. Toki, "LiV_3O_8: Characterization as Anode Material for an Aqueous Rechargeable Li-Ion Battery System," *Electrochim. Acta* **46** (2000) 59-65.

14. A. Eftekhari, "Electrochemical Behavior of Thin-film $LiMn_2O_4$ Electrode in Aqueous Media," *Electrochim. Acta* **47** (2001) 495-499.

15. J.W. Lee and S.I. Pyun, "Investigation of Lithium Transport Through $LiMn_2O_4$ Film Electrode in Aqueous $LiNO_3$ Solution," *Electrochim. Acta* **49** (2004) 753-761.

16. J.Y. Luo, W.J. Cui, P. He, and Y.Y. Xia, "Raising the Cycling Stability of Aqueous Lithium-ion Batteries by Eliminating Oxygen in the Electrolyte," *Nat. Chem.* **2** (2010) 760-765.

17. C.M. Burba and R. Frech, "Vibrational Spectroscopic Study of Lithium Intercalation into $LiTi_2(PO_4)_3$," *Solid State Ionics* **177** (2006) 1489-1494.

18. A.K. Padhi, K.S. Nanjundaswamy, and J.B. Goodenough, "Phospho-olivines as Positive-Electrode Materials for Rechargeable Lithium Batteries," *J. Electrochem. Soc.* **144** (1997) 1188-1194.

19. C. Delmas, A. Nadiri, and J.L. Soubeyroux, "The Nasicon-type Titanium Phosphates $ATi_2(PO_4)_3$ (A=Li, Na) as Electrode Materials," *Solid State Ionics* **28** (1988) 419-423.

20. G. Wang, L. Fu, N. Zhao, L. Yang, Y. Wu, and H. Wu, "An Aqueous Rechargeable Lithium Battery with Good Cycling Performance," *Angew. Chem. Int. Ed.* **46** (2007) 295-297.

21. Y.G.Wang and Y.Y. Xia, "A New Concept Hybrid Electrochemical Supercapacitor: Carbon/$LiMn_2O_4$ Aqueous System," *Electrochem. Commun.* **7** (2005) 1138-1142.

22. G.X.Wang, S. Zhong, D.H. Bradhurst, S.X. Dou, and H.K. Liu, "Secondary Aqueous Lithium-ion Batteries with Spinel Anodes and Cathodes," *J. Power Sources* **74** (1998) 198-201.

23. N.C. Li, C.J. Patrissi, G.L. Che, and C.R. Martin, "Rate Capabilities of Nanostructured $LiMn_2O_4$ Electrodes in Aqueous electrolyte," *J. Electrochem. Soc.* **147** (2000) 2044-2049.

24. X.H. Liu, T. Saito, T. Doi, S. Okada, and J. Yamaki, "Electrochemical Properties of Rechargeable Aqueous Lithium Ion Batteries with an Olivine-type Cathode and a Nasicon-type Anode," *J. Power Sources* **189** (2009) 706-710.

25. N.V. Kosova, D.I. Osintsev, N.F. Uvarov, and E.T. Devyatkina, "Lithium Titanium Phosphate as Cathode, Anode, and Electrolyte for Lithium Rechargeable Batteries," *Chem. Sustain. Dev.* **13** (2005) 253-260.

26. J.Y. Luo and Y.Y. Xia, "Aqueous Lithium-ion Battery LiTi2(PO4)3/LiMn2O4 with High Power and Energy Densities as well as Superior Cycling Stability," *Adv. Funct. Mater.* **17** (2007) 3877-3884.

27. H. Wang, K. Huang, Y. Zeng, S. Yang, and L. Chen, "Electrochemical Properties of TiP_2O_7 and $LiTi_2(PO_4)_3$ as Anode Material for Lithium Ion Battery with Aqueous Solution Electrolyte," *Electrochim. Acta* **52** (2007) 3280-3285.

28. R.B. Shivashankaraiah, H. Manjunatha, K.C. Mahesh, G.S. Suresh, and T.V. Venkatesha, "Electrochemical Characterization of $LiTi_2(PO_4)_3$ as Anode Material for Aqueous Rechargeable Lithium Batteries," *J. Electrochem. Soc.* **159** (2012) A1074-A1082.

29. H. Aono, E. Sugimoto, Y. Sadaoka, N. Imanaka, and G. Adachi, "Ionic Conductivity of the Lithium Titanium Phosphate ($Li_{1+x}M_xTi_{2-x}(PO_4)_3$, M=Al, Sc, Y, and La) Systems," *J. Electrochem. Soc.* **136** (1989) 590-591.

30. S.D. Jackman and R.A. Cutler, "Effect of Microcracking on Ionic Conductivity in LATP," *J. Power Sources* **218** (2012) 65-72.

31. A.V. Joshi, S. Balagopal, and J. Pendelton, "Electrolytic Method to Make Alkali Alcoholates Using Ion Conducting Alkali Electrolyte/Separator," U.S. Patent 8,075,758 (2011).

32. J.H. Gordon and S. Bhavaraju, "Device and Method for Recovery or Extraction of Lithium," U.S. Patent Application 20120103826 (2012).

33. M. Cretin, P. Fabry, and L. Abello, "Study of $Li_{1+x}Al_xTi_{2-x}(PO_4)_3$ for Li^+ Potentiometric Sensors," *J. Eur. Ceram. Soc.* **15** (1995) 1149-1156.

34. N. Imanishi, S. Hasegawa, T. Zhang, A. Hirano, Y. Takeda, and O. Yamamoto, "Lithium Anode for Lithium-air Secondary Batteries," *J. Power Sources* **185** (2008) 1392-1397.

35. T. Zhang, N. Imanishi, Y. Shimonishi, A. Hirano, Y. Takeda, O. Yamamoto, and N. Sammes, "A Novel High Energy Density Rechargeable Lithium/Air Battery," *Chem. Commun.* **46** (2010) 1661-1663.

36. S. Hasegawa, N. Imanishi, T. Zhang, J. Xie, A. Hirano, Y. Takeda, and O. Yamamoto, "Study on Lithium/Air Secondary Batteries–Stability of NASICON-type Lithium Ion Conducting Glass-ceramics with Water," *J. Power Sources* **189** (2009) 371-377.

37. T. Zhang, N. Imanishi, Y. Shimonishi, A. Hirano, J. Xie, Y. Takeda, O. Yamamoto, and N. Sammes, "Stability of a Water-Stable Lithium Metal Anode for a Lithium-Air Battery with Acetic Acid-Water Solutions," *J. Electrochem. Soc.* **157** (2010) A214-A218.

38. Y. Shimonishi, T. Zhang, N. Imanishi, D. Im, D.J. Lee, A. Hirano, Y. Takeda, O. Yamamoto, and N. Sammes, "A Study on Lithium/Air Secondary Batteries–Stability of NASICON-type Lithium Ion Conducting Solid Electrolyte in Alkaline Aqueous Solutions," *J. Power Sources* **196** (2011) 5128-5132.

39. ASTMC1499-09, Standard Test Method for Monotonic Equibiaxial Flexure Strength of Advanced Ceramics at Ambient Temperature, ASTM, Philadelphia, PA, 2009

40. J. Gulens, B.W. Hildebrandt, J.D. Canaday, A.K. Kuriakose, T.A. Wheat, and A. Ahmad, "Influence of Water on the Electrochemical Response of a Bonded Nasicon Protonic Conductor," *Solid State Ionics* **35** (1989) 45-49.

41. J.D. Canaday, S.F. Chehab, A.K. Kuriakose, A. Ahmad, and T.A. Wheat, "Protonic Conductivity of Hyceram^{TM}, a Bonded Hydronium NASICON," *Solid State Ionics* **48** (1991) 113-121.

42. P.G. Komorowski, S.A. Argyropoulos, R.G.V. Hancock, J. Gulens, P. Taylor, J.D. Canaday, A.K. Kuriakose, T.A. Wheat, and A. Ahmad, "Characterization of Protonically Exchanged NASICON," *Solid State Ionics* **48** (1991) 295-301.

43. R.O. Fuentes, F. Figueiredo, F.M.B. Marques, and J.I. Franco, "Reaction of NASICON with Water," *Solid State Ionics* **139** (2001) 309-314.

44. B.C. Bunker, G.W. Arnold, and J.A. Wilder, "Phosphate Glass Dissolution in Aqueous Solutions," *J. Non-Cryst. Solids* **64** (1984) 291-316.

45. Y.K. Lee and M. Tomozawa, "Effect of Water Content in Phosphate Glasses on Slow Crack Growth Rate," *J. Non-Cryst. Solids* **248** (1999) 203-210.

46. T.I. Suratwala, R.A. Steele, G.D. Wilke, J.H. Campbell, and K. Takeuchi, "Effects of OH Content, Water Vapor Pressure, and Temperature on Sub-critical Crack Growth in Phosphate Glass," *J. Non-Cryst. Solids* **263-264** (2000) 213-227.

47. A.V. Virkar, "A Model for Solid Oxide Fuel Cell (SOFC) Stack Degradation," *J. Power Sources* **172** (2007) 713-724.

48. A.V. Virkar, "Mechanism of Oxygen Electrode Delamination in Solid Oxide Electrolyzer Cells," *Int. J. Hydrogen Energy* **35** (2010) 9527-9543.

49. A.V. Virkar, "A Model for Degradation of Electrochemical Devices Based on Linear Non-equilibrium Thermodynamics and its Application to Lithium Ion Batteries," *J. Power Sources* **196** (2011) 5970-5984.

50. M.A. Laguna-Bercero, R. Campana, A. Larrea, J.A. Kilner, and V.M. Orera, "Electrolyte Degradation in Anode Supported Microtubular Yttria Stabilized Zirconia-based Solid Oxide Steam Electrolysis Cells at High Voltages of Operation," *J. Power Sources* **196** (2011) 8942-8947.

4. SUMMARY AND CONCLUSIONS

4.1 Microcracking

While the single-most important factor in increasing the ionic conductivity in LATP-based solid electrolytes is clearly the elimination of high-impedance secondary phases, which preferentially migrate to the grain boundaries, microcracking also lowers the conductivity of these materials when cracking is evident by Young's modulus measurements or using an SEM. Since the critical grain size for microcracking of $Li_{1.3}Al_{0.3}Ti_{1.7}P_3O_{12}$ is estimated to be less than 1.6 μm, very fine grains are required to avoid microcracked grain boundaries. The bulk conductivity was virtually constant between LATP that was phase-pure and LATP with secondary phases. The key to both improved strength and enhanced ionic conductivity in LATP materials will be processing a phase-pure ceramic with all grains below the critical size for microcracking.

The benefits of microcrack reduction were shown with thermal expansion, strength, and ionic conductivity measurements. The initial biaxial and flexural strengths measured were 123±17 MPa and 147±14 MPa, respectively, for phase-pure, high-purity, fine-grained LATP. While these strengths are still low for ionically conducting ceramics like cubic zirconia, they were more than double the strength of LATP with secondary phases. The bulk fracture toughness of LATP was measured to be 1.1±0.3 MPa√m, which allowed the defect size to be determined. Defects were on the order of 30 μm for

the best material and were not linked to microcracks, suggesting that further improvements in strength were possible. Subsequent samples obtained from Ceramatec had a biaxial strength in air of 144±13 MPa, equivalent to a flaw size of roughly 20 μm.

An important result of this work is the clear evidence that microcracking led to decreased conductivity due to increased impedance at grain boundaries. While no transmission electron microscopy was performed to determine if grain boundaries were devoid of secondary phases, comparison of similar purity materials clearly showed conductivity increasing with decreasing grain size. Increases in both conductivity and strength appear to be possible for LATP by a further reduction in grain size. High-purity, fine-grained LATP had the highest total ionic conductivity at all temperatures, measuring 0.67 mS cm^{-1} under ambient conditions with an activation energy of 0.35 eV. Improvements in grain boundary conductivity are not presumed to be an improvement in the actual conductivity of the material found at grain boundaries in LATP, but a reduction in void spaces through which Li-ions cannot be conducted. Although the observation of lowered ionic conductivity due to microcracking is intuitive, it has never been shown that microcracking is a serious concern for the ionic conductivity of LATP ceramics. Microcracking should be avoided not only from a strength perspective, but from the standpoint of ionic conductivity.

4.2 Strength Degradation in Presence of Moisture

High-purity, fine-grained LATP is susceptible to stress-corrosion cracking, with strength decreasing dramatically (191 MPa to 26 MPa) when exposed to water. The strength in salt solutions was highly correlated with the ability of water to solvate the salt, with LiOH showing the highest strength (76 MPa) in static solutions. In the case of

LiOH, static testing showed that LATP could last for hundreds of hours in the same high pH (>11.5) that resulted in short-term cathodic pitting in electrochemical testing. It was also shown that changes in strength can be a more sensitive indicator of degradation than XRD and a.c. impedance measurements, evidenced here by the results of LATP in aqueous LiOH solutions.

4.3 LATP as a Solid Electrolyte in Aqueous Media

When tested at the same Li^+ concentration (2 wt%) and current density (25 mA cm^{-2}) at 40°C in deionized water, $LiNO_3$ and LiOH solutions resulted in the highest conductivity in LATP membranes (~1.8 mS cm^{-1}) while LiCl was slightly lower (~1.5 mS cm^{-1}) and $LiCOOCH_3$ had the lowest conductivity (~1.1 mS cm^{-1}). Electrode reactions resulted in high pH at the cathode and low pH at the anode, both of which are problematic for LATP. However, by using a common flask, which allowed for self-buffering in the case of $LiCOOCH_3$, it was possible to show that the LATP was stable over hundreds of hours of operation in the pH range of 8–9.

In order for LATP to be used in aqueous solutions in electrochemical cells, two conditions must be satisfied for low-temperature (40-60°C) operation: 1) the pH must be maintained in the range of 7–10, and 2) the Na^+ concentration must be kept low to avoid ion exchange. There are no practical applications for LATP in aqueous solutions, but strength testing in mineral oil suggests that it may be worthwhile to look at this material in nonprotonic organic solvents used for electrochemical cells.